SUPPORTING INFORMATION

Metal-cyanido molecular modulators of the sensing range and performance in lanthanide-based luminescent thermometers

Maciej Wyczesany, Jakub J. Zakrzewski, Barbara Sieklucka, and Szymon Chorazy*

Faculty of Chemistry, Jagiellonian University, Gronostajowa 2, 30-387 Kraków, Poland

*Corresponding author: simon.chorazy@uj.edu.pl

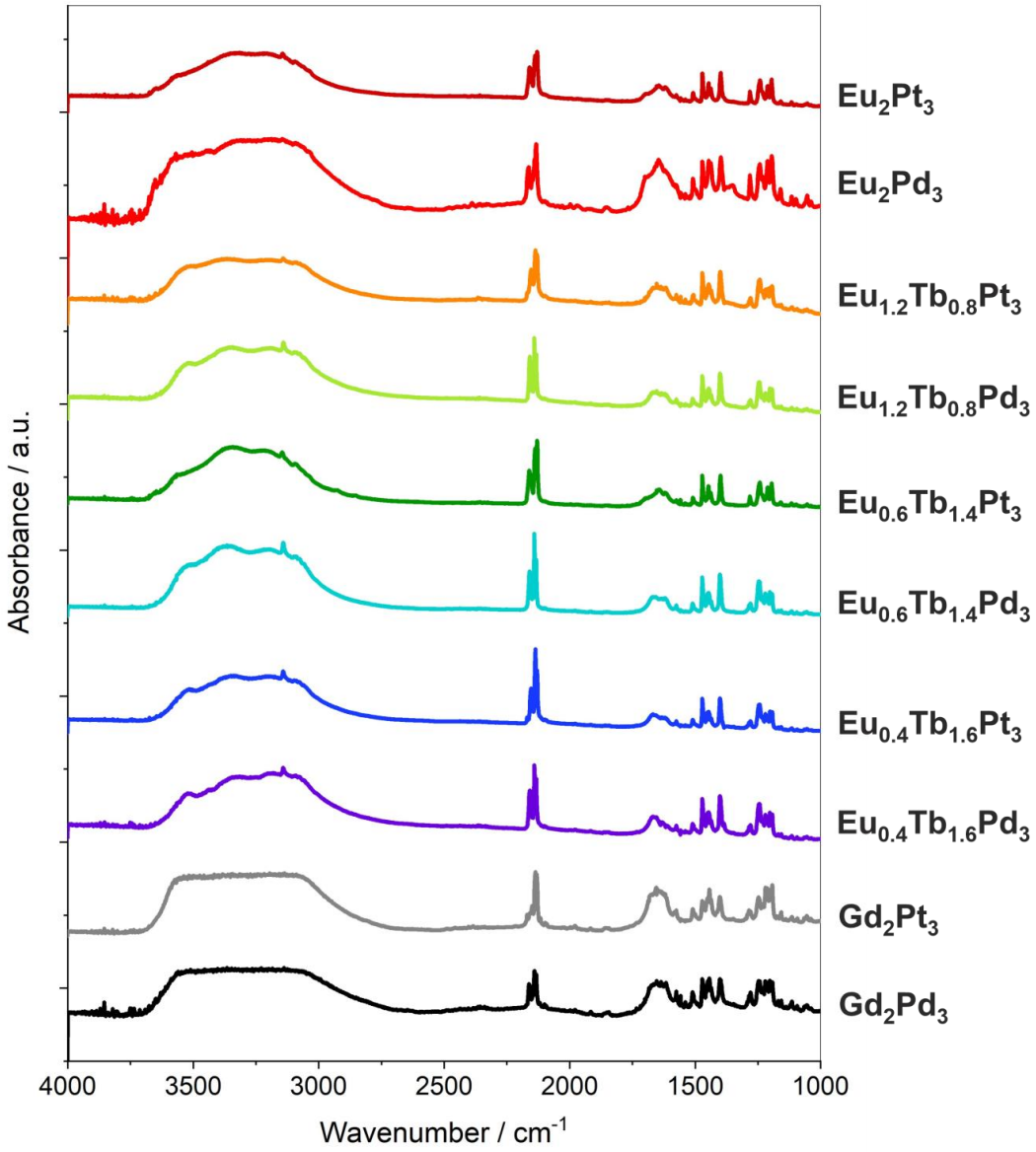

Fig. S1 Infrared (IR) absorption spectra of the selected single crystals of **Eu_2M_3**, **$Eu_{1.2}Tb_{0.8}M_3$**, **$Eu_{0.6}Tb_{1.4}M_3$**, **$Eu_{0.4}Tb_{1.6}M_3$**, and **Gd_2M_3** (M = Pt, Pd) materials, gathered in the 1000–4000 cm^{-1} wavenumber range.

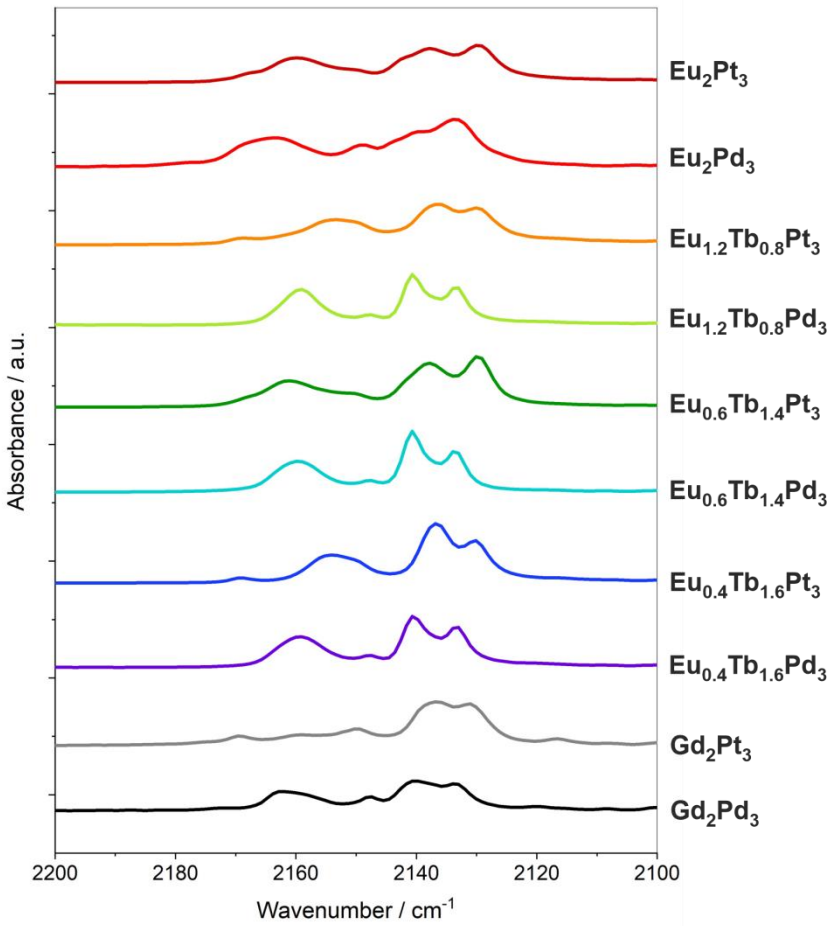

Fig. S2 Infrared (IR) absorption spectra of the selected single crystals of **Eu_2M_3**, **$Eu_{1.2}Tb_{0.8}M_3$**, **$Eu_{0.6}Tb_{1.4}M_3$**, **$Eu_{0.4}Tb_{1.6}M_3$**, and **Gd_2M_3** (M = Pt, Pd) materials shown in the limited 2100–2200 cm^{-1} wavenumber range related to the stretching vibrations of cyanido ligands.[S1,S2]

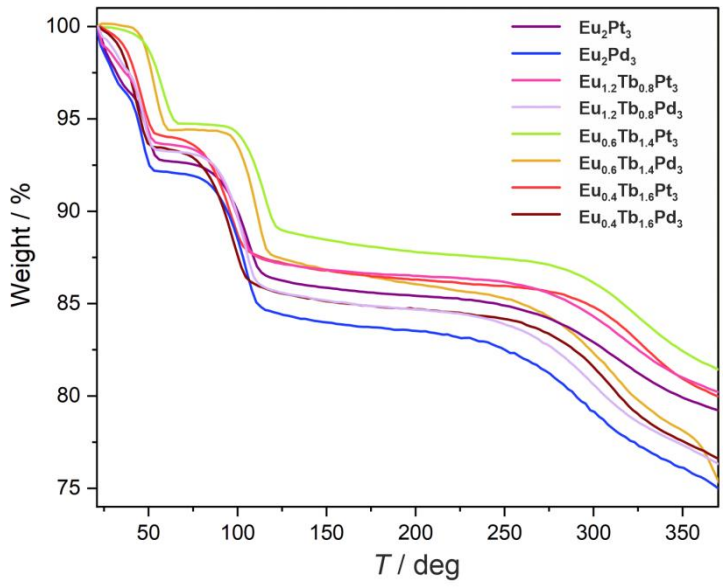

Fig. S3 The view of superimposed thermogravimetric curves of **Eu_2M_3**, **$Eu_{1.2}Tb_{0.8}M_3$**, **$Eu_{0.6}Tb_{1.4}M_3$**, and **$Eu_{0.4}Tb_{1.6}M_3$** (M = Pt, Pd), collected in the temperature range of 20–370°C. The experiments were conducted under a nitrogen atmosphere with a heating rate of 1°C per minute.

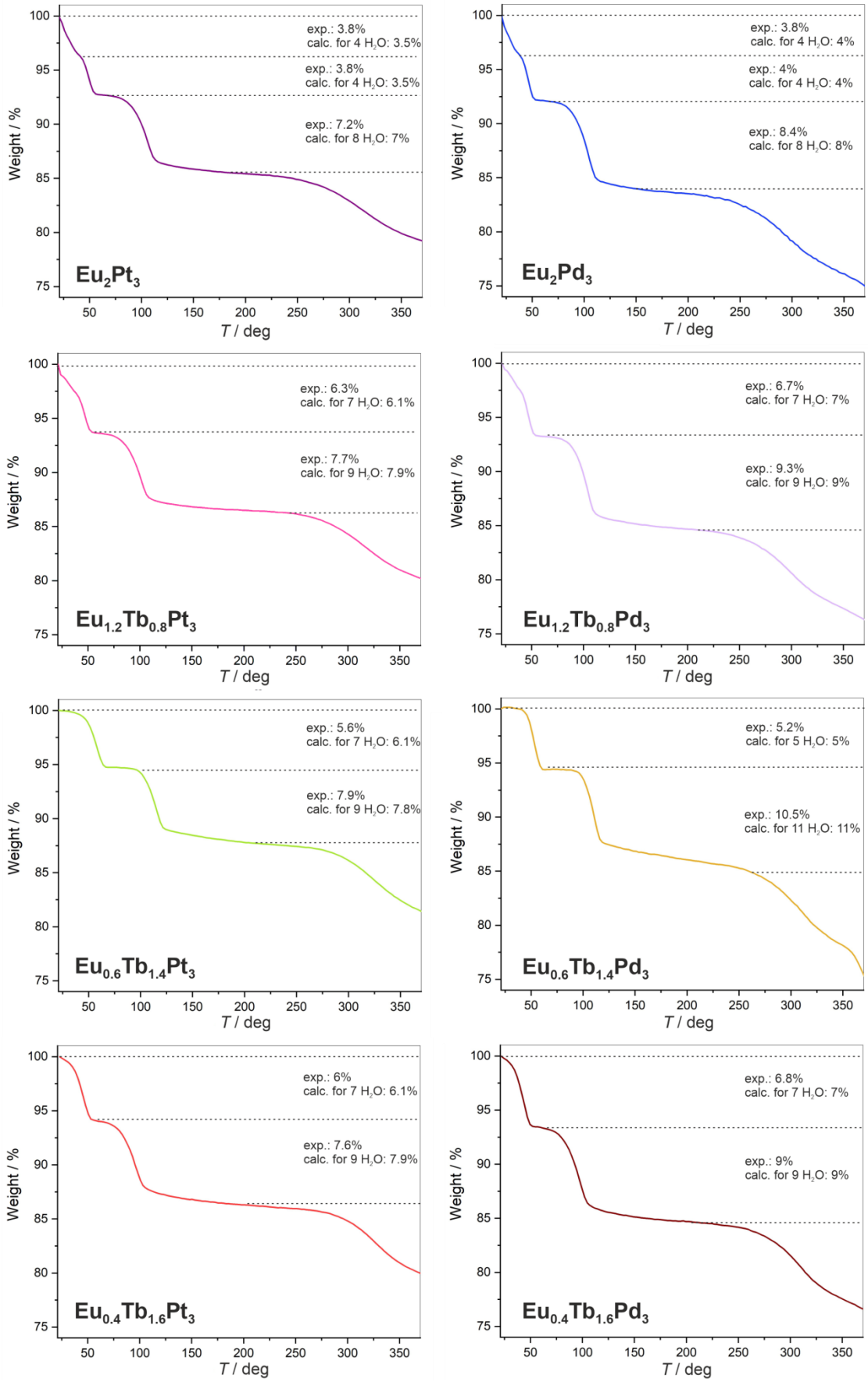

Fig. S4 Thermogravimetric curves of Eu_2M_3, $Eu_{1.2}Tb_{0.8}M_3$, $Eu_{0.6}Tb_{1.4}M_3$, and $Eu_{0.4}Tb_{1.6}M_3$ (M = Pt, Pd), collected in the temperature range of 20–370°C. The steps related to the loss of water molecules are depicted. The experiments were conducted under a nitrogen atmosphere with a heating rate of 1°C per minute.

Table S1 Crystal data and structure refinement for **Eu_2Pt_3**, **Eu_2Pd_3**, and **$Eu_{1.2}Tb_{0.8}Pt_3$**.

compound		**Eu_2Pt_3**	**Eu_2Pd_3**	**$Eu_{1.2}Tb_{0.8}Pt_3$**
method		single-crystal XRD		
formula		$C_{42}H_{54}Eu_2N_{18}O_{22}Pt_3$	$C_{42}H_{54}Eu_2N_{18}O_{22}Pd_3$	$C_{42}H_{54}Eu_{1.2}N_{18}O_{22}Pt_3Tb_{0.8}$
formula weight / g·mol^{-1}		2052.22	1786.15	2057.79
T / K		100(2)		
λ / Å		0.71075		
crystal system		monoclinic		
space group		$P\,2_1/n$		
unit cell	a / Å	11.4490(7)	11.4556(5)	11.4393(14)
	b / Å	22.1355(14)	22.2459(10)	22.166(3)
	c / Å	12.8194(8)	12.8259(7)	12.8011(16)
	α / deg	90	90	90
	β / deg	105.8930(10)	106.6880(10)	106.162(2)
	γ / deg	90	90	90
V / Å^3		3124.6(3)	3130.9(3)	3117.6(7)
Z		2	2	2
calculated density / g·cm^{-3}		2.181	1.895	2.192
absorption coefficient / cm^{-1}		8.755	2.904	8.878
F(000)		1936	1744	1939
crystal size / mm × mm × mm		0.15 × 0.15 × 0.12	0.33 × 0.12 × 0.07	0.18 × 0.14 × 0.13
crystal type		colourless block		
θ range / deg		2.609–25.791	2.607–27.099	2.610–25.045
limiting indices		-12 < h < 13 -27 < k < 27 -15 < l < 15	-14 < h < 14 -16 < k < 28 -16 < l < 16	-13 < h < 13 -26 < k < 20 -15 < l < 15
collected reflections		18099	18835	14107
unique reflections		5973	6875	5516
R_{int}		0.0463	0.0282	0.0518
completeness / %		99.9	99.5	99.7
max. and min. transmission		0.5151 and 0.7453	0.5316 and 0.7455	0.4601 and 0.7453
data/restraints/parameters		5973/58/454	6875/40/459	5516/87/457
GOF on F^2		1.017	1.050	1.016
final R indices		R_1 = 0.0321 [$I > 2\sigma(I)$] wR_2 = 0.0633 (all)	R_1 = 0.0248 [$I > 2\sigma(I)$] wR_2 = 0.0541 (all)	R_1 = 0.0372 [$I > 2\sigma(I)$] wR_2 = 0.0682 (all)
largest diff peak/hole / e·Å^{-3}		2.409/–2.243	1.033/–0.580	2.027/–1.502

Table S2 Crystal data and structure refinement for **$Eu_{1.2}Tb_{0.8}Pd_3$**, **$Eu_{0.6}Tb_{1.4}Pt_3$**, and **$Eu_{0.6}Tb_{1.4}Pd_3$**.

compound		**$Eu_{1.2}Tb_{0.8}Pd_3$**	**$Eu_{0.6}Tb_{1.4}Pt_3$**	**$Eu_{0.6}Tb_{1.4}Pd_3$**
method		single-crystal XRD		
formula		$C_{42}H_{54}Eu_{1.2}N_{18}O_{22}Pd_3Tb_{0.8}$	$C_{42}H_{54}Eu_{0.6}N_{18}O_{22}Pt_3Tb_{1.4}$	$C_{42}H_{54}Eu_{0.6}N_{18}O_{22}Pd_3Tb_{1.4}$
formula weight / g·mol^{-1}		1791.72	2061.96	1795.89
T / K		100(2)		
λ / Å		0.71075		
crystal system		Monoclinic		
space group		$P\ 2_1/n$		
unit cell	a / Å	11.4179(12)	11.472(6)	11.4547(5)
	b / Å	22.231(2)	22.330(13)	22.3063(9)
	c / Å	12.7888(13)	12.850(7)	12.8111(5)
	α / deg	90	90	90
	β / deg	106.892(2)	106.334(18)	107.0240(10)
	γ / deg	90	90	90
V / Å^3		3106.1(5)	3159(3)	3130.0(2)
Z		2	2	2
calculated density / g·cm^{-3}		1.916	2.168	1.906
absorption coefficient / cm^{-1}		3.03	8.838	3.084
F(000)		1747	1942	1750
crystal size / mm × mm × mm		0.16 × 0.16 × 0.11	0.24 × 0.23 × 0.13	0.26 × 0.19 × 0.13
crystal type		colourless block		
θ range / deg		2.614–27.101	2.786–26.253	2.834–27.101
limiting indices		-14 < h < 14 -28 < k < 28 -16 < l < 16	-14 < h < 14 -27< k < 26 -15 < l < 15	-12 < h < 14 -28< k < 28 -16 < l < 16
collected reflections		20621	22378	19552
unique reflections		6820	6355	6896
R_{int}		0.0634	0.0427	0.0366
completeness / %		99.7	99.8	99.8
max. and min. transmission		0.5150 and 0.7455	0.4836 and 0.7457	0.5828 and 0.7459
data/restraints/parameters		6820/22/458	6355/34/459	6896/46/459
GOF on F^2		1.040	1.040	1.016
final R indices		R_1 = 0.0478 [$I > 2\sigma(I)$] wR_2 = 0.1312 (all)	R_1 = 0.0291 [$I > 2\sigma(I)$] wR_2 = 0.0619 (all)	R_1 = 0.0281 [$I > 2\sigma(I)$] wR_2 = 0.0538 (all)
largest diff peak/hole / e·Å^{-3}		1.662/–1.774	1.878/–1.585	1.225/–0.583

Table S3 Crystal data and structure refinement for **$Eu_{0.4}Tb_{1.6}Pt_3$**, **$Eu_{0.4}Tb_{1.6}Pd_3$**, and **Tb_2Pt_3**.

compound		**$Eu_{0.4}Tb_{1.6}Pt_3$**	**$Eu_{0.4}Tb_{1.6}Pd_3$**	**Tb_2Pt_3**
method		single-crystal XRD		
formula		$C_{42}H_{54}Eu_{0.4}N_{18}O_{22}Pt_3Tb_{1.6}$	$C_{42}H_{54}Eu_{0.4}N_{18}O_{22}Pd_3Tb_{1.6}$	$C_{42}H_{54}N_{18}O_{22}Pt_3Tb_2$
formula weight / g·mol^{-1}		2063.35	1797.28	2066.14
T / K		100(2)		
λ / Å		0.71075		
crystal system		monoclinic		
space group		$P\,2_1/n$		
unit cell	a / Å	11.4222(4)	11.4463(11)	11.542(4)
	b / Å	22.1905(8)	22.294(2)	22.358(9)
	c / Å	12.7908(4)	12.8057(12)	12.815(5)
	α / deg	90	90	90
	β / deg	106.3420(10)	107.063(2)	106.046(8)
	γ / deg	90	90	90
V / Å^3		3111.03(18)	3123.9(5)	3178(2)
Z		2	2	2
calculated density / g·cm^{-3}		2.203	1.911	2.159
absorption coefficient / cm^{-1}		8.998	3.116	8.860
F(000)		1942	1750	1944
crystal size / mm × mm × mm		0.11 × 0.11 × 0.07	0.28 × 0.18 × 0.17	0.19 × 0.18 × 0.17
crystal type		colourless block		
θ range / deg		2.305–24.900	2.785–25.682	2.587–25.026
limiting indices		-13 < h < 13 -26 < k < 26 -15 < l < 15	-12 < h < 13 -27< k < 25 -15 < l < 15	-11< h < 13 -26< k < 26 -15 < l < 14
collected reflections		26309	11737	15092
unique reflections		5414	5908	5487
R_{int}		0.0413	0.0326	0.1374
completeness / %		99.8	99.6	97.9
max. and min. transmission		0.5894 and 0.7451	0.6117 and 0.7453	0.2787 and 0.7452
data/restraints/parameters		5414/22/459	5908/22/459	5487/71/451
GOF on F^2		1.040	1.015	1.031
final R indices		R_1 = 0.0239 [$I > 2\sigma(I)$] wR_2 = 0.0472 (all)	R_1 = 0.0294 [$I > 2\sigma(I)$] wR_2 = 0.0644 (all)	R_1 = 0.1124 [$I > 2\sigma(I)$] wR_2 = 0.2783 (all)
largest diff peak/hole / e·Å^{-3}		1.342/–1.194	1.236/–1.021	4.322/–2.323

Table S4 Crystal data and structure refinement for **Gd_2Pt_3** and **Gd_2Pd_3**.

compound		**Gd_2Pt_3**	**Gd_2Pd_3**
method		single-crystal XRD	
formula		$C_{42}H_{54}Gd_2N_{18}O_{22}Pt_3$	$C_{42}H_{54}Gd_2N_{18}O_{22}Pd_3$
formula weight / g·mol^{-1}		2062.80	1796.73
T / K		100(2)	
λ / Å		0.71075	
crystal system		monoclinic	
space group		$P\ 2_1/n$	
unit cell	a / Å	11.4148(16)	11.4690(9)
	b / Å	22.138(3)	22.2703(18)
	c / Å	12.7885(18)	12.8290(10)
	α / deg	90	90
	β / deg	106.140(3)	106.840(2)
	γ / deg	90	90
V / Å^3		3104.2(7)	3136.2(4)
Z		2	2
calculated density / g·cm^{-3}		2.207	1.903
absorption coefficient / cm^{-1}		8.929	3.014
F(000)		1940	1748
crystal size / mm × mm × mm		0.19 × 0.04 × 0.09	0.19 × 0.15 × 0.05
crystal type		colourless block	
θ range / deg		2.615–27.098	2.469–27.103
limiting indices		-12 < h < 14 -28 < k < 28 -16 < l < 16	-14 < h < 14 -28< k < 28 -16 < l < 16
collected reflections		18933	34955
unique reflections		6835	6921
R_{int}		0.0712	0.0421
completeness / %		99.9	99.9
max. and min. transmission		0.5623 and 0.7458	0.5990 and 0.7459
data/restraints/parameters		6835/65/454	6921/65/454
GOF on F^2		0.999	1.019
final R indices		R_1 = 0.0435 [$I > 2\sigma(I)$] wR_2 = 0.0841 (all)	R_1 = 0.0264 [$I > 2\sigma(I)$] wR_2 = 0.0596 (all)
largest diff peak/hole / e·Å^{-3}		2.114/–1.805	1.088/–0.826

Table S5 Detailed metric parameters of lanthanide(III) complexes in **Eu_2Pt_3**, **Eu_2Pd_3**, and **$Eu_{1.2}Tb_{0.8}Pt_3$**.

parameter	Eu_2Pt_3	Eu_2Pd_3	$Eu_{1.2}Tb_{0.8}Pt_3$
Ln1-Ln1’	4.3040(6) Å	4.2969(3) Å	4.2955(8) Å
Ln1-O1	2.446(4) Å	2.443(2) Å	2.426(5) Å
Ln1-O2	2.467(4) Å	2.452(2) Å	2.456(5) Å
Ln1-O3	2.464(4) Å	2.461(2) Å	2.452(5) Å
Ln1-O4	2.396(4) Å	2.390(2) Å	2.379(5) Å
Ln1-O5	2.392(4) Å	2.387(2) Å	2.382(5) Å
Ln1-O6	2.419(4) Å	2.419(2) Å	2.407(5) Å
Ln1-O7	2.483(5) Å	2.483(2) Å	2.478(6) Å
Ln1-N1	2.487(5) Å	2.488(3) Å	2.478(6) Å
O1-Ln1-O2	66.52(14)°	66.35(7)°	66.71(17)°
O1-Ln1-O3	67.30(14)°	85.12(7)°	85.14(17)°
O1-Ln1-O4	78.96(15)°	79.19(8)°	78.99(18)°
O1-Ln1-O5	136.09(15)°	136.34(7)°	136.58(18)°
O1-Ln1-O6	137.39(15)°	137.40(8)°	137.27(17)°
O1-Ln1-O7	139.00(15)°	138.75(8)°	138.97(18)°
O1-Ln1-N1	78.50(16)°	78.37(8)°	78.2(2)°
O2-Ln1-O3	69.67°	69.64(7)°	69.75(16)°
O2-Ln1-O4	68.56(14)°	68.38(8)°	68.37(18)°
O2-Ln1-O5	69.58(15)°	69.99(7)°	69.88(18)°
O2-Ln1-O6	132.07(15)°	132.42(8)°	132.30(18)°
O2-Ln1-O7	125.82(15)°	126.16(8)°	125.76(17)°
O2-Ln1-N1	135.21(16)°	135.07(8)°	135.3(2)°
O3-Ln1-O4	138.23(14)°	138.01(7)°	138.12(18)°
O3-Ln1-O5	80.37(14)°	80.55(8)°	80.70(18)°
O3-Ln1-O6	72.44(15)°	72.75(8)°	72.69(18)°
O3-Ln1-O7	135.24(15)°	135.55(8)°	135.33(19)°
O3-Ln1-N1	135.81(15)°	135.61(8)°	135.39(18)°
O4-Ln1-O5	84.78(16)°	84.49(8)°	84.8(2)°
O4-Ln1-O6	140.41(15)°	140.17(8)°	140.39(19)°
O4-Ln1-O7	72.84(16)°	72.78(8)°	72.96(19)°
O4-Ln1-N1	78.30(16)°	78.72(8)°	78.7(2)°
O5-Ln1-O6	76.15(16)°	76.08(8)°	76.04(19)°
O5-Ln1-O7	70.43(15)°	70.54(8)°	70.10(19)°
O5-Ln1-N1	137.32(16)°	137.29(9)°	137.3(2)°
O6-Ln1-O7	68.18(16)°	68.06(8)°	68.01(19)°
O6-Ln1-N1	92.62(17)°	92.40(9)°	92.3(2)°
O7-Ln1-N1	67.21(17)°	67.04(9)°	67.4(2)°

Table S6 Detailed metric parameters of $[M^{II}(CN)_4]^{2-}$ (M = Pt, Pd) complexes in **Eu_2Pt_3**, **Eu_2Pd_3**, and **$Eu_{1.2}Tb_{0.8}Pt_3$**.

parameter	Eu_2Pt_3	Eu_2Pd_3	$Eu_{1.2}Tb_{0.8}Pt_3$
M1-C1	1.981(6) Å	1.978(3) Å	1.984(8) Å
M1-C21	2.007(7) Å	2.006(3) Å	1.995(8) Å
M2-C2	1.986(7) Å	1.998(4) Å	1.992(9) Å
M2-C3	2.000(9) Å	1.992(5) Å	1.990(10) Å
M2-C4	1.997(7) Å	1.995(4) Å	1.986(9) Å
M2-C5	1.960(8) Å	1.986(5) Å	1.967(10) Å
C1-M1-C21	91.0(3)°	91.10(14)°	91.2(3)°
C1-M1-C1’	180°	180°	180°
C21-M1-C21’	180°	180°	180°
C2-M2-C3	91.9(3)°	91.75(16)°	91.7(4)°
C2-M2-C4	177.2(3)°	177.69(16)°	177.2(4)°
C2-M2-C5	87.8(3)°	87.71(15)°	86.9(3)°
C3-M2-C4	90.0(3)°	89.72(16)°	90.1(4)°
C3-M2-C5	178.3(3)°	179.23(17)°	178.2(4)°
C4-M2-C5	90.3(3)°	90.84(16)°	91.3(4)°

Table S7 Detailed metric parameters of lanthanide(III) complexes in $Eu_{1.2}Tb_{0.8}Pd_3$, $Eu_{0.6}Tb_{1.4}Pt_3$, and $Eu_{0.6}Tb_{1.4}Pd_3$.

parameter	$Eu_{1.2}Tb_{0.8}Pd_3$	$Eu_{0.6}Tb_{1.4}Pt_3$	$Eu_{0.6}Tb_{1.4}Pd_3$
Ln1-Ln1’	4.2805(8) Å	4.308(2) Å	4.2910(3) Å
Ln1-O1	2.417(5) Å	2.437(4) Å	2.426(2) Å
Ln1-O2	2.442(5)Å	2.462(4) Å	2.442(2) Å
Ln1-O3	2.442(5) Å	2.456(4) Å	2.440(2) Å
Ln1-O4	2.372(5) Å	2.384(4) Å	2.372(2) Å
Ln1-O5	2.368(5) Å	2.381(4) Å	2.369(2) Å
Ln1-O6	2.402(5) Å	2.411(4) Å	2.402(2) Å
Ln1-O7	2.467(6) Å	2.487(4) Å	2.473(3) Å
Ln1-N1	2.471(6) Å	2.486(5) Å	2.471(3) Å
O1-Ln1-O2	66.19(17)°	66.53(12)°	66.55(8)°
O1-Ln1-O3	84.99(17)°	85.32(12)°	85.38(8)°
O1-Ln1-O4	79.26(17)°	78.87(13)°	79.25(8)°
O1-Ln1-O5	136.29(18)°	136.49(12)°	136.73(8)°
O1-Ln1-O6	137.21(17)°	137.21(12)°	137.06(8)°
O1-Ln1-O7	138.95(19)°	138.85(12)°	138.69(8)°
O1-Ln1-N1	78.22(19)°	78.06(13)°	78.19(9)°
O2-Ln1-O3	69.43(16)°	69.70(12)°	69.93(8)°
O2-Ln1-O4	68.22(17)°	68.45(12)°	68.22(8)°
O2-Ln1-O5	70.11(18)°	69.97(13)°	70.18(8)°
O2-Ln1-O6	132.80(18)°	132.73(13)°	132.84(8)°
O2-Ln1-O7	126.22(18)°	126.08(12)°	126.15(8)°
O2-Ln1-N1	135.1(2)°	135.08(14)°	135.21(9)°
O3-Ln1-O4	137.64(17)°	138.14(12)°	138.14(8)°
O3-Ln1-O5	80.77(17)°	80.63(13)°	80.60(8)°
O3-Ln1-O6	73.09(18)°	72.87(13)°	72.69(8)°
O3-Ln1-O7	135.51(19)°	135.24(13)°	135.29(8)°
O3-Ln1-N1	135.18(18)°	135.40(13)°	135.23(8)°
O4-Ln1-O5	84.05(19)°	84.73(14)°	84.47(9)°
O4-Ln1-O6	140.21(18)°	140.36(13)°	140.22(9)°
O4-Ln1-O7	72.9(2)°	73.07(14)°	72.88(9)°
O4-Ln1-N1	79.41(19)°	78.63(14)°	79.13(9)°
O5-Ln1-O6	76.55(19)°	76.44(13)°	76.31(9)°
O5-Ln1-O7	70.23(19)°	70.25(13)°	70.37(9)°
O5-Ln1-N1	137.5(2)°	137.41(14)°	137.30(9)°
O6-Ln1-O7	67.9(2)°	67.82(14)°	67.96(9)°
O6-Ln1-N1	91.9(2)°	92.05(14)°	91.81(9)°
O7-Ln1-N1	67.6(2)°	67.46(14)°	67.17(9)°

Table S8 Detailed metric parameters of $[M^{II}(CN)_4]^{2-}$ (M = Pt, Pd) complexes in $\mathbf{Eu_{1.2}Tb_{0.8}Pd_3}$, $\mathbf{Eu_{0.6}Tb_{1.4}Pt_3}$, and $\mathbf{Eu_{0.6}Tb_{1.4}Pd_3}$.

parameter	$\mathbf{Eu_{1.2}Tb_{0.8}Pd_3}$	$\mathbf{Eu_{0.6}Tb_{1.4}Pt_3}$	$\mathbf{Eu_{0.6}Tb_{1.4}Pd_3}$
M1-C1	1.975(7) Å	1.984(5) Å	1.982(3) Å
M1-C21	2.013(8) Å	2.014(6) Å	2.004(4) Å
M2-C2	1.990(10) Å	2.007(6) Å	1.998(4) Å
M2-C3	1.973(12) Å	2.002(7) Å	1.994(5) Å
M2-C4	1.999(10) Å	2.008(6) Å	1.999(4) Å
M2-C5	1.981(10) Å	1.992(7) Å	1.989(5) Å
C1-M1-C21	90.9(3)°	90.9(2)°	91.38(15)°
C1-M1-C1’	180°	180°	180°
C21-M1-C21’	180°	180°	180°
C2-M2-C3	92.2(4)°	91.4(3)°	91.69(16)°
C2-M2-C4	177.9(4)°	177.3(3)°	177.78(17)°
C2-M2-C5	87.7(4)°	87.9(3)°	87.70(16)°
C3-M2-C4	89.1(4)°	90.3(3)°	89.64(17)°
C3-M2-C5	179.4(4)°	178.8(3)°	179.31(17)°
C4-M2-C5	91.0(4)°	90.4(3)°	90.98(17)°

Table S9 Detailed metric parameters of lanthanide(III) complexes in **$Eu_{0.4}Tb_{1.6}Pt_3$**, **$Eu_{0.4}Tb_{1.6}Pd_3$**, and **Tb_2Pt_3**.

parameter	$Eu_{0.4}Tb_{1.6}Pt_3$	$Eu_{0.4}Tb_{1.6}Pd_3$	Tb_2Pt_3
Ln1-Ln1’	4.2878(5) Å	4.2864(5) Å	4.32 Å
Ln1-O1	2.423(3) Å	2.417(3) Å	2.43(2) Å
Ln1-O2	2.448(3) Å	2.444(3) Å	2.435(18) Å
Ln1-O3	2.438(3) Å	2.438(3) Å	2.455(19) Å
Ln1-O4	2.368(3) Å	2.365(3) Å	2.39(2) Å
Ln1-O5	2.362(3) Å	2.364(3) Å	2.38(2) Å
Ln1-O6	2.399(3) Å	2.398(3) Å	2.38(2) Å
Ln1-O7	2.472(4) Å	2.469(3) Å	2.52(2) Å
Ln1-N1	2.467(4) Å	2.467(4) Å	2.49(3) Å
O1-Ln1-O2	66.75(11)°	66.58(10)°	68.2(6)°
O1-Ln1-O3	85.54(11)°	85.48(10)°	85.2(7)°
O1-Ln1-O4	78.81(12)°	79.28(11)°	81.1(8)°
O1-Ln1-O5	136.62(11)°	136.69(10)°	137.4(7)°
O1-Ln1-O6	137.29(11)°	137.02(10)°	138.1(8)°
O1-Ln1-O7	138.66(12)°	138.40(11)°	139.2(7)°
O1-Ln1-N1	78.04(13)°	77.97(11)°	78.2(8)°
O2-Ln1-O3	69.85(11)°	69.94(10)°	70.3(7)°
O2-Ln1-O4	68.47(11)°	68.44(10)°	68.7(7)°
O2-Ln1-O5	69.88(12)°	70.12(10)°	69.2(8)°
O2-Ln1-O6	132.65(12)°	132.83(10)°	131.0(8)°
O2-Ln1-O7	125.97(12)°	126.06(10)°	124.6(8)°
O2-Ln1-N1	135.35(13)°	135.04(11)°	135.4(9)°
O3-Ln1-O4	138.32(11)°	138.37(10)°	139.0(7)°
O3-Ln1-O5	80.72(11)°	80.49(10)°	81.8(7)°
O3-Ln1-O6	72.76(12)°	72.62(10)°	72.6(8)°
O3-Ln1-O7	135.18(12)°	135.50(10)°	135.0(8)°
O3-Ln1-N1	135.22(12)°	135.25(11)°	136.1(8)°
O4-Ln1-O5	84.69(13)°	84.58(11)°	82.7(8)°
O4-Ln1-O6	140.28(12)°	140.15(11)°	137.8(8)°
O4-Ln1-O7	73.00(13)°	72.48(11)°	71.5(9)°
O4-Ln1-N1	78.77(13)°	78.85(11)°	78.2(9)°
O5-Ln1-O6	76.41(12)°	76.38(11)°	74.9(8)°
O5-Ln1-O7	70.21(12)°	70.55(11)°	69.0(8)°
O5-Ln1-N1	137.32(13)°	137.51(12)°	135.7(9)°
O6-Ln1-O7	67.82(12)°	68.26(11)°	67.3(9)°
O6-Ln1-N1	91.87(13)°	91.98(12)°	93.6(10)°
O7-Ln1-N1	67.39(13)°	67.20(11)°	67.1(9)°

Table S10 Detailed metric parameters of $[M^{II}(CN)_4]^{2-}$ (M = Pt, Pd) complexes in **$Eu_{0.4}Tb_{1.6}Pt_3$**, **$Eu_{0.4}Tb_{1.6}Pd_3$**, and **Tb_2Pt_3**.

parameter	$Eu_{0.4}Tb_{1.6}Pt_3$	$Eu_{0.4}Tb_{1.6}Pd_3$	Tb_2Pt_3
M1-C1	1.981(5) Å	1.981(4) Å	1.96(3) Å
M1-C21	2.001(5) Å	2.007(4) Å	1.99(3) Å
M2-C2	1.995(6) Å	2.005(5) Å	2.03(4) Å
M2-C3	1.998(7) Å	1.992(6) Å	1.91(6) Å
M2-C4	1.997(6) Å	1.996(5) Å	1.97(5) Å
M2-C5	1.976(7) Å	1.984(6) Å	1.98(5) Å
C1-M1-C21	91.0(2)°	91.17(19)°	90.3(14)°
C1-M1-C1’	180°	180°	180°
C21-M1-C21’	180°	180°	180°
C2-M2-C3	91.7(2)°	91.6(2)°	92(2)°
C2-M2-C4	177.4(2)°	177.8(2)°	174(2)°
C2-M2-C5	87.6(2)°	87.9(2)°	86(2)°
C3-M2-C4	90.0(2)°	89.6(2)°	93(2)°
C3-M2-C5	178.4(3)°	179.4(2)°	177(2)°
C4-M2-C5	90.7(2)°	90.9(2)°	89.0(19)°

Table S11 Detailed metric parameters of lanthanide(III) complexes in **Gd_2Pt_3** and **Gd_2Pd_3**.

parameter	Gd_2Pt_3	Gd_2Pd_3
Ln1-Ln1’	4.286(5) Å	4.294(5) Å
Ln1-O1	2.439(5) Å	2.439(2) Å
Ln1-O2	2.454(5) Å	2.446(2)Å
Ln1-O3	2.447(5) Å	2.455(2) Å
Ln1-O4	2.382(5) Å	2.385(2) Å
Ln1-O5	2.368(6) Å	2.373(2) Å
Ln1-O6	2.422(5) Å	2.411(2) Å
Ln1-O7	2.471(6) Å	2.478(2) Å
Ln1-N1	2.474(6) Å	2.477(3) Å
O1-Ln1-O2	66.98(17) °	66.58(7)°
O1-Ln1-O3	85.50(18)°	85.24(7)°
O1-Ln1-O4	79.23(19)°	79.29(8)°
O1-Ln1-O5	136.38(18)°	136.43(8)°
O1-Ln1-O6	137.40(19)°	137.19(8)°
O1-Ln1-O7	138.86(18)°	138.58(8)°
O1-Ln1-N1	78.2(2)°	78.25(8)°
O2-Ln1-O3	69.56(17)°	69.79(7)°
O2-Ln1-O4	68.59(18)°	68.31(8)°
O2-Ln1-O5	69.40(18)°	69.85(8)°
O2-Ln1-O6	132.20(18)°	132.57(8)°
O2-Ln1-O7	125.87(19)°	125.91(8)°
O2-Ln1-N1	135.5(2)°	135.27(8)°
O3-Ln1-O4	138.14(18)°	138.08(7)°
O3-Ln1-O5	80.25(19)°	80.64(8)°
O3-Ln1-O6	72.77(18)°	72.72(8)°
O3-Ln1-O7	135.06(18)°	135.60(8)°
O3-Ln1-N1	135.9(2)°	135.30(8)°
O4-Ln1-O5	84.5(2)°	84.31(8)°
O4-Ln1-O6	139.95(19)°	140.16(8)°
O4-Ln1-O7	72.85(19)°	72.57(8)°
O4-Ln1-N1	78.6(2)°	79.04(8)°
O5-Ln1-O6	76.2(2)°	76.37(8)°
O5-Ln1-O7	70.5(2)°	70.49(8)°
O5-Ln1-N1	137.3(2)°	137.39(9)°
O6-Ln1-O7	67.72(19)°	68.23(8)°
O6-Ln1-N1	92.3(2)°	92.03(9)°
O7-Ln1-N1	67.2(2)°	67.16(9)°

Table S12 Detailed metric parameters of $[M^{II}(CN)_4]^{2-}$ (M = Pt, Pd) complexes in **Gd_2Pt_3** and **Gd_2Pd_3**.

parameter	Gd_2Pt_3	Gd_2Pd_3
M1-C1	1.985(7) Å	1.977(3)Å
M1-C21	2.003(9) Å	2.005(4) Å
M2-C2	1.999(9) Å	2.002(4) Å
M2-C3	1.997(11) Å	1.992(5) Å
M2-C4	2.003(9) Å	1.994(4) Å
M2-C5	1.979(9) Å	1.986(4) Å
C1-M1-C21	91.1(3)°	91.18(14)°
C1-M1-C1’	180°	180°
C21-M1-C21’	180°	180°
C2-M2-C3	91.9(4)°	92.03(16)°
C2-M2-C4	176.9(4)°	177.49(16)°
C2-M2-C5	87.5(4)°	87.39(16)°
C3-M2-C4	90.3(4)°	89.49(16)°
C3-M2-C5	178.6(4)°	179.27(16)°
C4-M2-C5	90.4(4)°	91.11(16)°

Table S13 Results of Continuous Shape Measure (CSM)[S3,S4] analysis for $[Ln(terpyO_3)(H_2O)_4(NC)]^{2+}$ complexes in the crystal structure of **Eu_2M_3**, **$Eu_{1.2}Tb_{0.8}M_3$**, **$Eu_{0.6}Tb_{1.4}M_3$**, **$Eu_{0.4}Tb_{1.6}M_3$**, **Tb_2Pt_3**, and **Gd_2M_3** (M = Pt, Pd).

compound	CSM parameters*			geometry
	CSAPR-9	TCTPR-9	JCSAPR-9	
Eu_2Pt_3	0.762	0.602	1.703	intermediate TCTPR-9 / CSAPR-9
Eu_2Pd_3	0.753	0.622	1.710	intermediate TCTPR-9 / CSAPR-9
$Eu_{1.2}Tb_{0.8}Pt_3$	0.779	0.616	1.707	intermediate TCTPR-9 / CSAPR-9
$Eu_{1.2}Tb_{0.8}Pd_3$	0.776	0.657	1.701	intermediate TCTPR-9 / CSAPR-9
$Eu_{0.6}Tb_{1.4}Pt_3$	0.784	0.618	1.707	intermediate TCTPR-9 / CSAPR-9
$Eu_{0.6}Tb_{1.4}Pd_3$	0.803	0.637	1.738	intermediate TCTPR-9 / CSAPR-9
$Eu_{0.4}Tb_{1.6}Pt_3$	0.811	0.620	1.728	intermediate TCTPR-9 / CSAPR-9
$Eu_{0.4}Tb_{1.6}Pd_3$	0.803	0.622	1.724	intermediate TCTPR-9 / CSAPR-9
Tb_2Pt_3	0.795	0.735	1.775	intermediate TCTPR-9 / CSAPR-9
Gd_2Pt_3	0.780	0.612	1.706	intermediate TCTPR-9 / CSAPR-9
Gd_2Pd_3	0.776	0.630	1.733	intermediate TCTPR-9 / CSAPR-9

* CSM parameters:
CSM CSAPR-9 = the parameter related to the capped square antiprism (C_{4v} symmetry)
CSM TCTPR-9 = the parameter related to the tricapped trigonal prism (D_{3h} symmetry)
CSM JCSAPR-9 = the parameter related to the capped square antiprism, gyroelongated square pyramid J10 (C_{4v} symmetry)
CSM = 0 for the ideal geometry and the increase of CSM parameter corresponds to the increasing distortion from the ideal polyhedron.

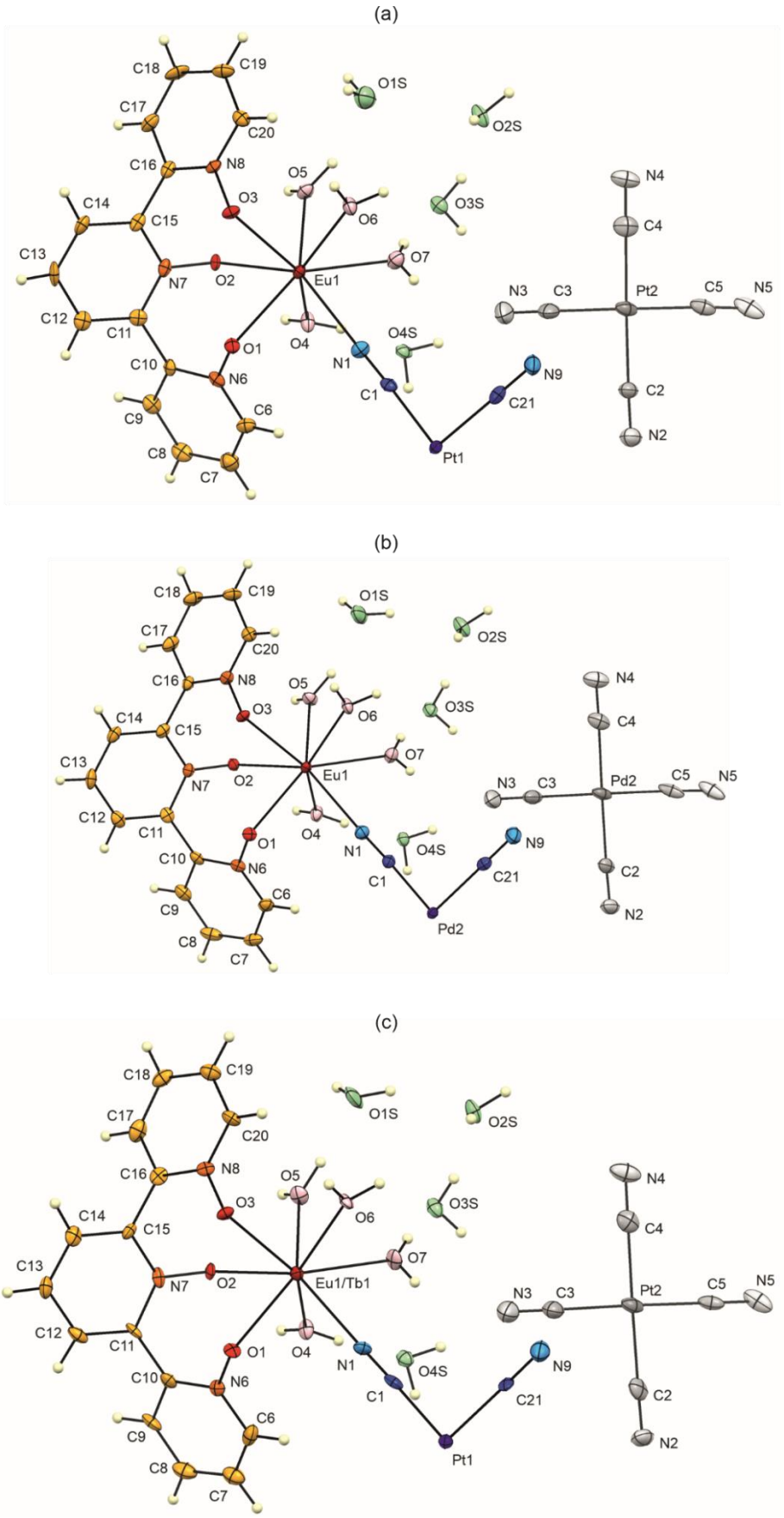

Fig. S5 Asymmetric units of Eu_2Pt_3 (a), Eu_2Pd_3 (b), and $Eu_{1.2}Tb_{0.8}Pt_3$ (c) with the atoms labeling schemes. Thermal ellipsoids are presented at the 50% probability level. The related bond lengths and angles are collected in Tables S5 and S6.

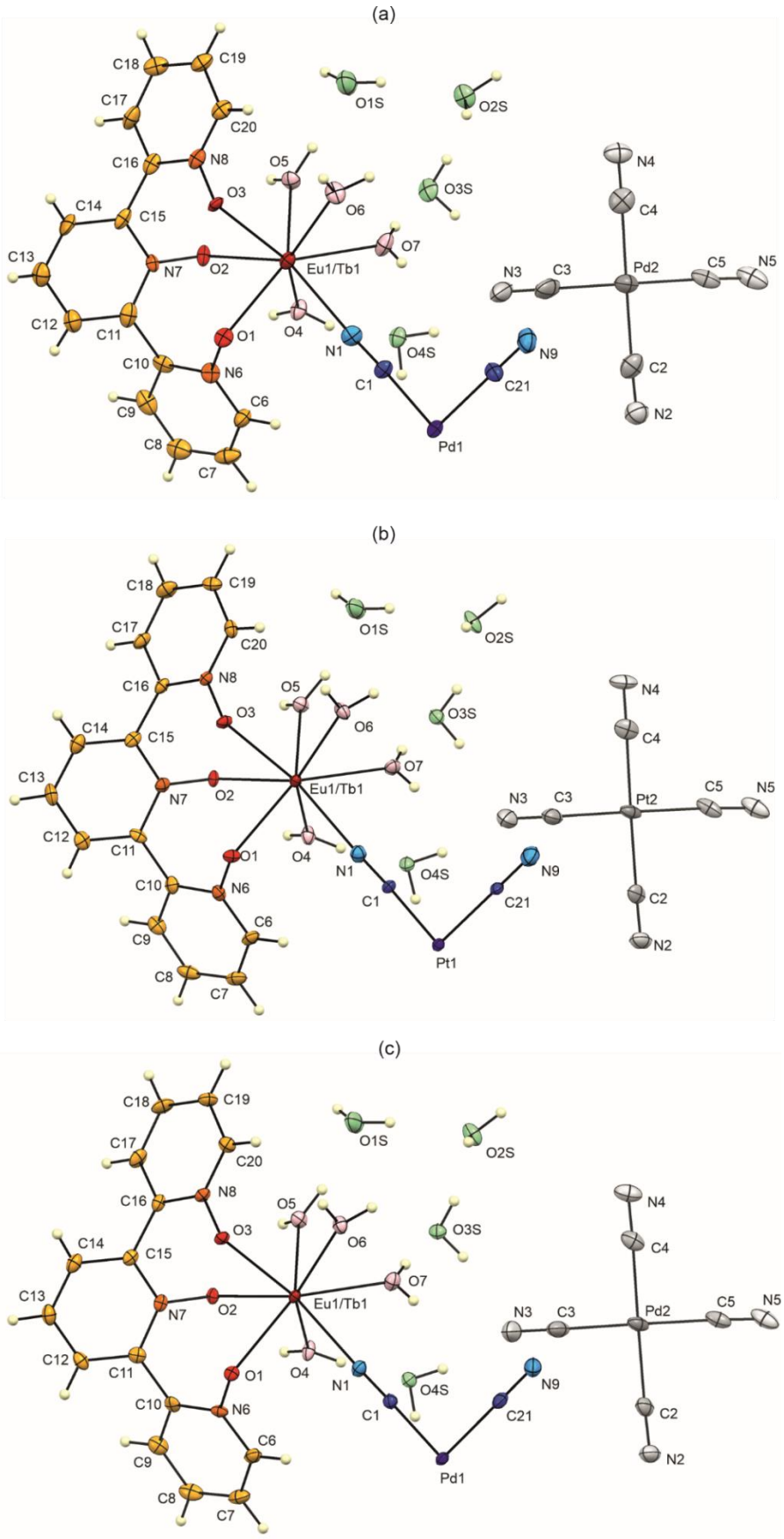

Fig. S6 Asymmetric units of $\mathbf{Eu_{1.2}Tb_{0.8}Pd_3}$ (a), $\mathbf{Eu_{0.6}Tb_{1.4}Pt_3}$ (b), and $\mathbf{Eu_{0.6}Tb_{1.4}Pd_3}$ (c) with the atoms labeling schemes. Thermal ellipsoids are presented at the 50% probability level. The related bond lengths and angles are collected in Tables S7 and S8.

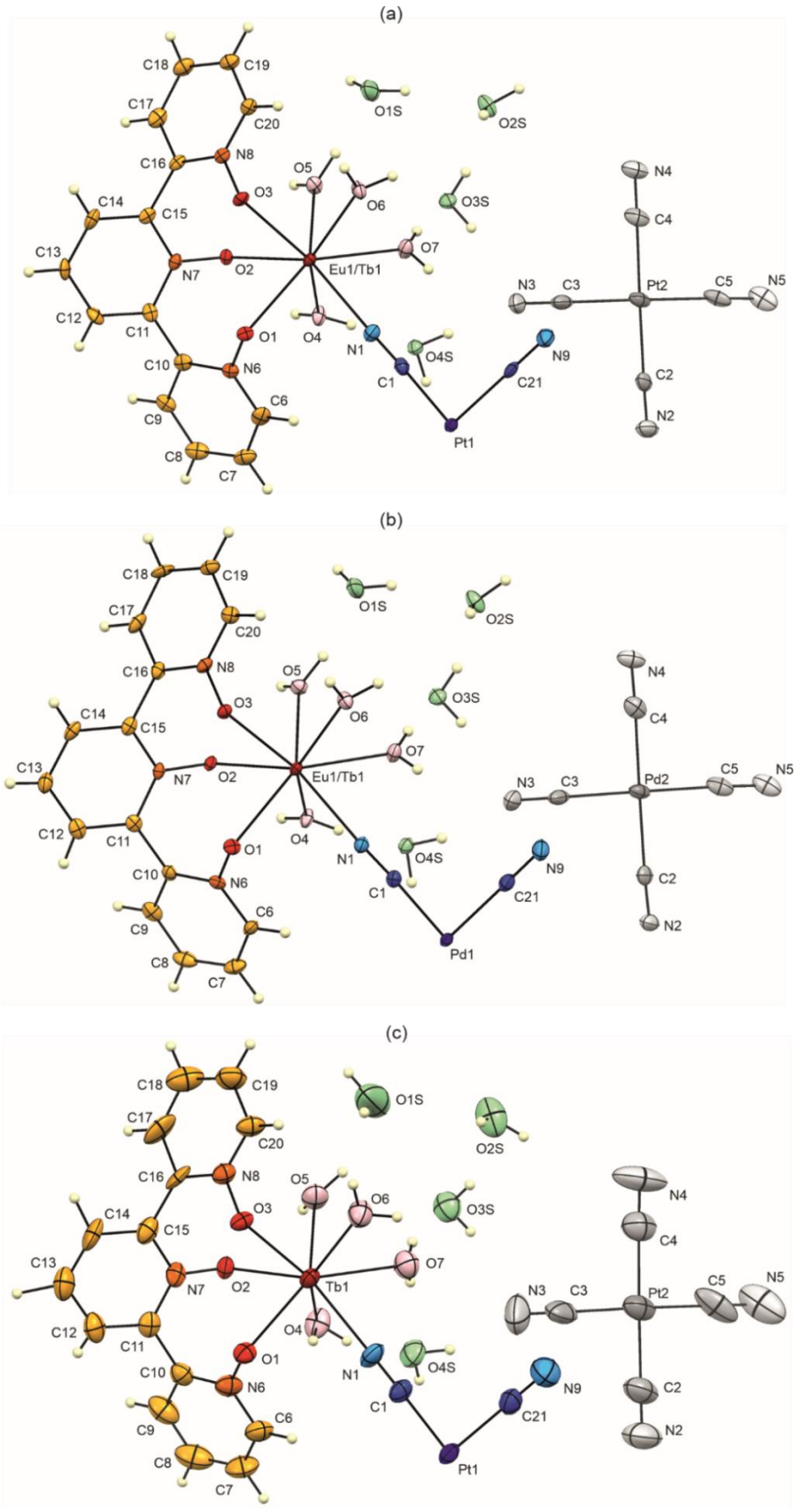

Fig. S7 Asymmetric units of $\mathbf{Eu_{0.4}Tb_{1.6}Pt_3}$ (a), $\mathbf{Eu_{0.4}Tb_{1.6}Pd_3}$ (b), and $\mathbf{Tb_2Pt_3}$ (c) with the atoms labeling schemes. Thermal ellipsoids are presented at the 50% probability level. The related bond lengths and angles are collected in Tables S9 and S10.

(a)

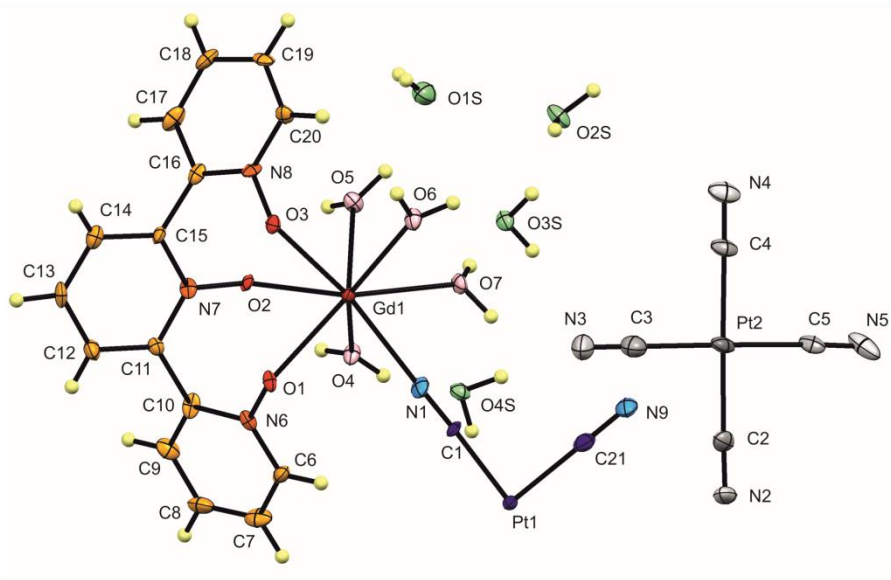

(b)

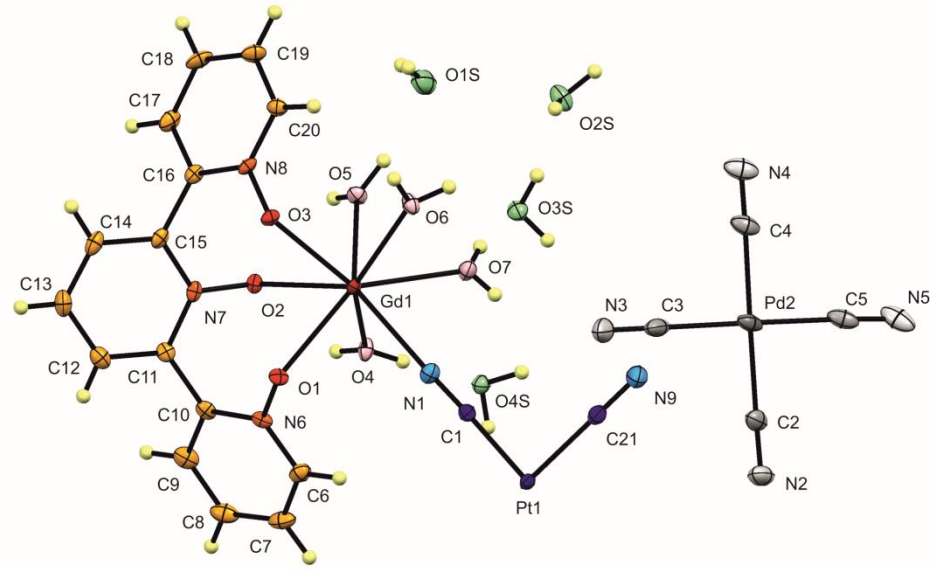

Fig. S8 Asymmetric units of **Gd_2Pt_3** (a) and **Gd_2Pd_3** (b) with the atoms labeling schemes. Thermal ellipsoids are presented at the 50% probability level. The related bond lengths and angles are collected in Tables S11 and S12.

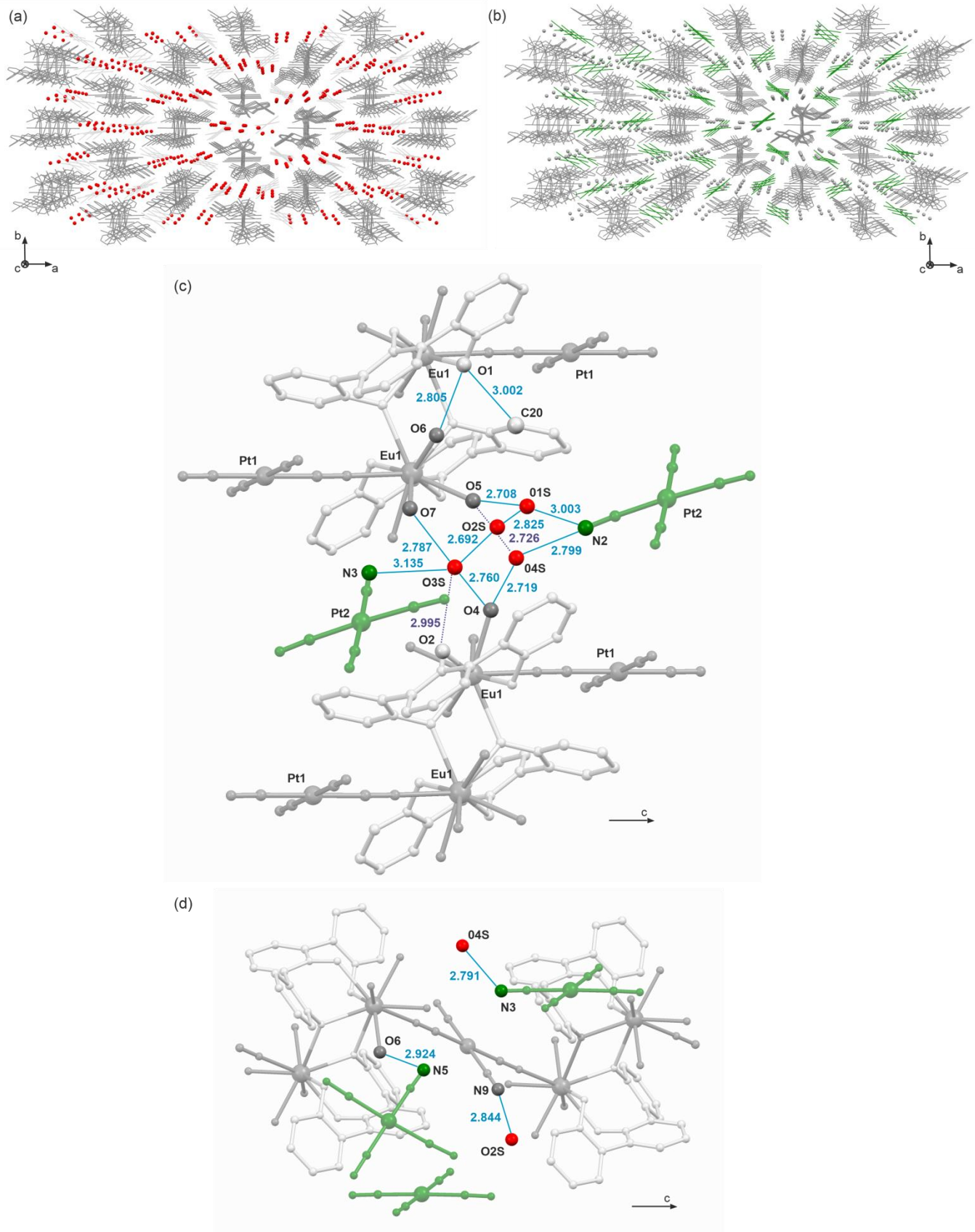

Fig. S9 Arrangement of crystallization water molecules (a, water molecules are shown as red balls) and non-coordinated tetracyanidometallate(II) counter-ions (b, cyanido complexes are green coloured) in the supramolecular network of **Eu_2Pt_3**, and the detailed views of the related hydrogen bonds network shown for two representative fragments of the structure (c, d). The supramolecular network of other reported compounds is analogous.

Table S14 Donor-acceptor distances of the hydrogen bonding network of **Eu_2Pt_3**, **Eu_2Pd_3**, and **$Eu_{1.2}Tb_{0.8}Pt_3$** (see Fig. S9 for comparison).

donor-H···acceptor	Eu_2Pt_3	Eu_2Pd_3	$Eu_{1.2}Tb_{0.8}Pt_3$
O1S-H1B···N2	3.003(8) Å	3.011(4) Å	3.002(10) Å
O5-H5B···O4S	2.726(6) Å	2.714(3) Å	2.727(8) Å
C20-H20··· O1	3.002(8) Å	3.001(4) Å	2.999(9) Å
O2S-H2A···N9	2.842(7) Å	2.858(4) Å	2.878(9) Å
O3S-H3A···O2S	2.694(7) Å	2.714(3) Å	2.691(8) Å
O2S-H2B··· N5	2.848(8) Å	2.859(4) Å	2.850(9) Å
O7-H7A···O3S	2.766(7) Å	2.759(3) Å	2.759(8) Å
O3S-H3B···O2	2.994(6) Å	3.033(3) Å	3.003(8) Å
O3S-H3B···N3	3.135(8) Å	3.057(4) Å	3.097(10) Å
O6-H6B···O1	2.805(6) Å	2.804(3) Å	2.809(7) Å
O6-H6A···N5	2.924(8) Å	2.910(4) Å	2.906(9) Å
O4-H4D···O4S	2.718(6) Å	2.725(3) Å	2.722(7) Å
O4-H4C···O3S	2.760(6) Å	2.772(3) Å	2.764(8) Å
O4S-H4A···N2	2.800(7) Å	2.793(4) Å	2.781(9) Å
O5-H5C···O1S	2.709(7) Å	2.708(3) Å	2.689(8) Å
O4S-H4F···N3	2.791(8) Å	2.795(4) Å	2.793(10) Å

Table S15 Donor-acceptor distances in the hydrogen bonding network of **$Eu_{1.2}Tb_{0.8}Pd_3$**, **$Eu_{0.6}Tb_{1.4}Pt_3$**, and **$Eu_{0.6}Tb_{1.4}Pd_3$** (see Fig. S9 for comparison).

donor-H···acceptor	$Eu_{1.2}Tb_{0.8}Pd_3$	$Eu_{0.6}Tb_{1.4}Pt_3$	$Eu_{0.6}Tb_{1.4}Pd_3$
O1S-H1B···N2	3.003(10) Å	3.018(7) Å	3.013(4) Å
O5-H5B···O4S	2.712(7) Å	2.734(5) Å	2.722(3) Å
C20-H20··· O1	3.003(9) Å	3.023(7) Å	3.003(4) Å
O2S-H2A···N9	2.870(9) Å	2.879(7) Å	2.871(4) Å
O3S-H3A···O2S	2.712(8) Å	2.722(6) Å	2.720(4) Å
O2S-H2B··· N5	2.850(9) Å	2.874(7) Å	2.875(4) Å
O7-H7A···O3S	2.752(8) Å	2.784(6) Å	2.771(4) Å
O3S-H3B···O2	3.028(7) Å	3.011(5) Å	3.035(3) Å
O3S-H3B···N3	3.031(10) Å	3.113(7) Å	3.042(5) Å
O6-H6B···O1	2.801(7) Å	2.825(5) Å	2.808(3) Å
O6-H6A···N5	2.906(9) Å	2.927(7) Å	2.915(4) Å
O4-H4D···O4S	2.725(7) Å	2.734(5) Å	2.727(3) Å
O4-H4C···O3S	2.767(8) Å	2.779(5) Å	2.775(4) Å
O4S-H4A···N2	2.793(10) Å	2.812(6) Å	2.804(4) Å
O5-H5C···O1S	2.703(8) Å	2.715(6) Å	2.709(4) Å
O4S-H4F···N3	2.788(11) Å	2.811(7) Å	2.797(4) Å

Table S16 Donor-acceptor distances in the hydrogen bonding network of **$Eu_{0.4}Tb_{1.6}Pt_3$**, **$Eu_{0.4}Tb_{1.6}Pd_3$**, and **Tb_2Pt_3** (see Fig. S9 for comparison).

donor-H···acceptor	$Eu_{0.4}Tb_{1.6}Pt_3$	$Eu_{0.4}Tb_{1.6}Pd_3$	Tb_2Pt_3
O1S-H1B···N2	2.996(6) Å	3.008(5) Å	3.08(7) Å
O5-H5B···O4S	2.727(5) Å	2.719(4) Å	2.76(3) Å
C20-H20··· O1	2.996(6) Å	2.999(5) Å	3.02(4) Å
O2S-H2A···N9	2.857(6) Å	2.872(5) Å	2.94(5) Å
O3S-H3A···O2S	2.713(5) Å	2.723(5) Å	2.74(4) Å
O2S-H2B··· N5	2.852(6) Å	2.870(5) Å	2.87(5) Å
O7-H7A···O3S	2.769(5) Å	2.763(5) Å	2.77(4) Å
O3S-H3B···O2	2.995(5) Å	3.036(4) Å	3.03(4) Å
O3S-H3B···N3	3.098(6) Å	3.041(6) Å	3.16(6) Å
O6-H6B···O1	2.820(5) Å	2.807(5) Å	2.86(3) Å
O6-H6A···N5	2.911(6) Å	2.910(5) Å	2.88(5) Å
O4-H4D···O4S	2.715(5) Å	2.725(4) Å	2.76(3) Å
O4-H4C···O3S	2.761(5) Å	2.789(4) Å	2.80(3) Å
O4S-H4A···N2	2.799(6) Å	2.799(5) Å	2.75(4) Å
O5-H5C···O1S	2.700(5) Å	2.708(4) Å	2.68(6) Å
O4S-H4F···N3	2.788(6) Å	2.791(6) Å	2.84(6) Å

Table S17 Donor-acceptor distances in the hydrogen bonding network of **Gd_2Pt_3** and **Gd_2Pd_3**.

donor-H···acceptor	**Gd_2Pt_3**	**Gd_2Pd_3**
O1S-H1B···N2	3.018(7) Å	3.020(4) Å
O5-H5B···O4S	2.734(5) Å	2.725(3) Å
C20-H20··· O1	3.023(7) Å	2.999(4) Å
O2S-H2A···N9	2.879(7) Å	2.866(4) Å
O3S-H3A···O2S	2.722(6) Å	2.720(4) Å
O2S-H2B··· N5	2.875(7) Å	2.871(4) Å
O7-H7A···O3S	2.784(6) Å	2.765(4) Å
O3S-H3B···O2	3.011(5) Å	3.036(3) Å
O3S-H3B···N3	3.113(7) Å	3.051(4) Å
O6-H6B···O1	2.825(5) Å	2.806(3) Å
O6-H6A···N5	2.927(7) Å	2.914(4) Å
O4-H4D···O4S	2.734(5) Å	2.721(3) Å
O4-H4C···O3S	2.779(5) Å	2.777(3) Å
O4S-H4A···N2	2.812(6) Å	2.794(4) Å
O5-H5C···O1S	2.715(6) Å	2.723(4) Å
O4S-H4F···N3	2.811(7) Å	2.797(4) Å

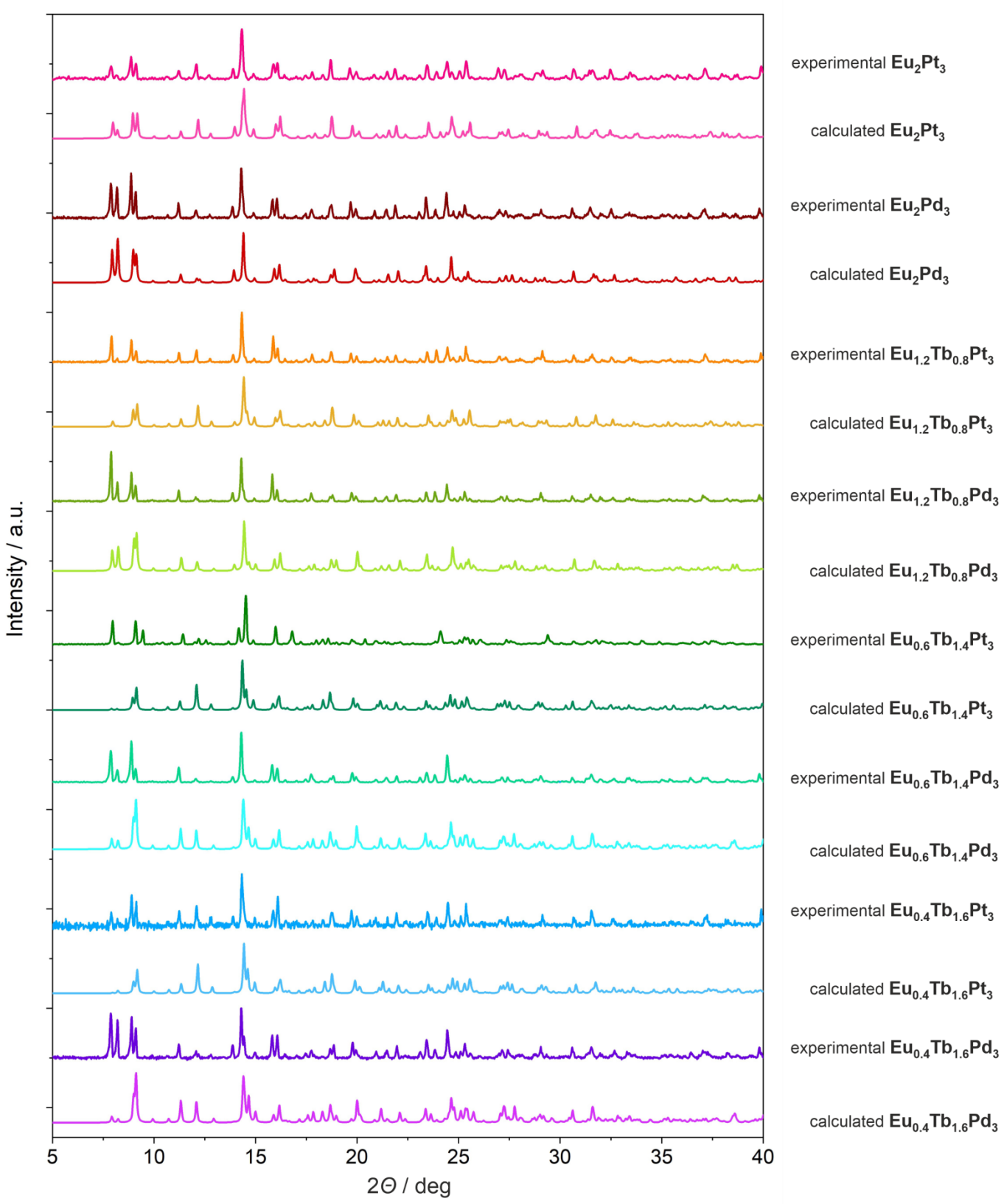

Fig. S10 Experimental powder X-ray diffraction (P-XRD) patterns of the polycrystalline samples of Eu_2M_3, $Eu_{1.2}Tb_{0.8}M_3$, $Eu_{0.6}Tb_{1.4}M_3$, and $Eu_{0.4}Tb_{1.6}M_3$ (M = Pt, Pd) materials, compared with the P-XRD patterns calculated from the respective structural models obtained within the single-crystal X-ray diffraction (SC-XRD) analyses.

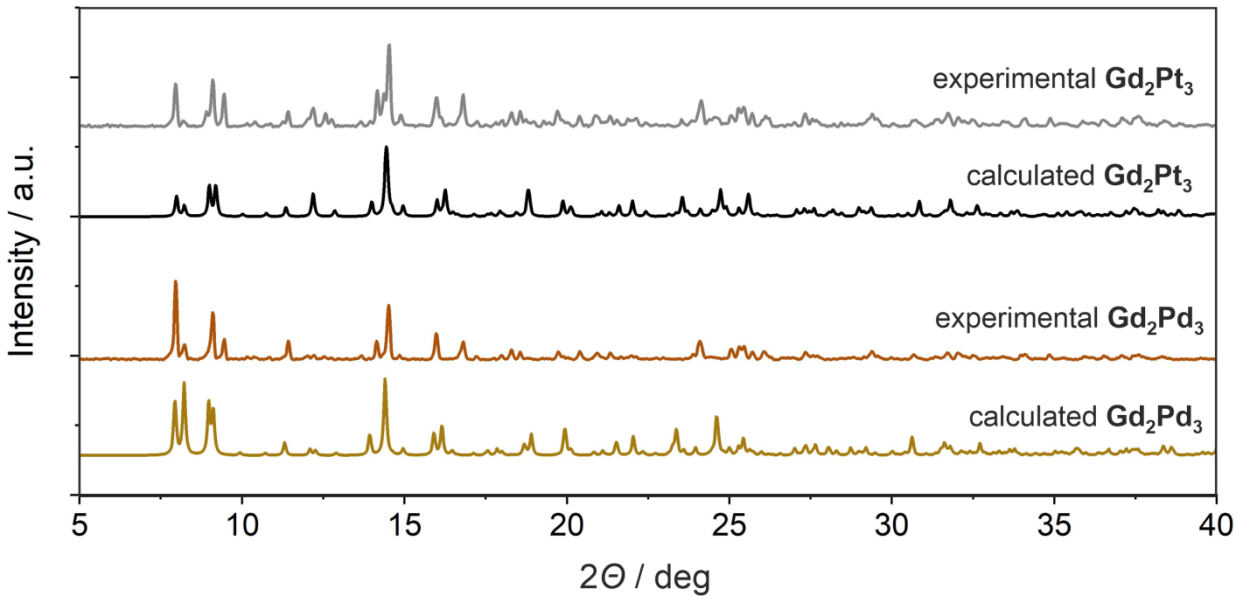

Fig. S11 Experimental P-XRD patterns of the polycrystalline samples of **Gd_2Pt_3** and **Gd_2Pd_3** materials, compared with the P-XRD patterns calculated from the respective structural models obtained within the SC-XRD analyses.

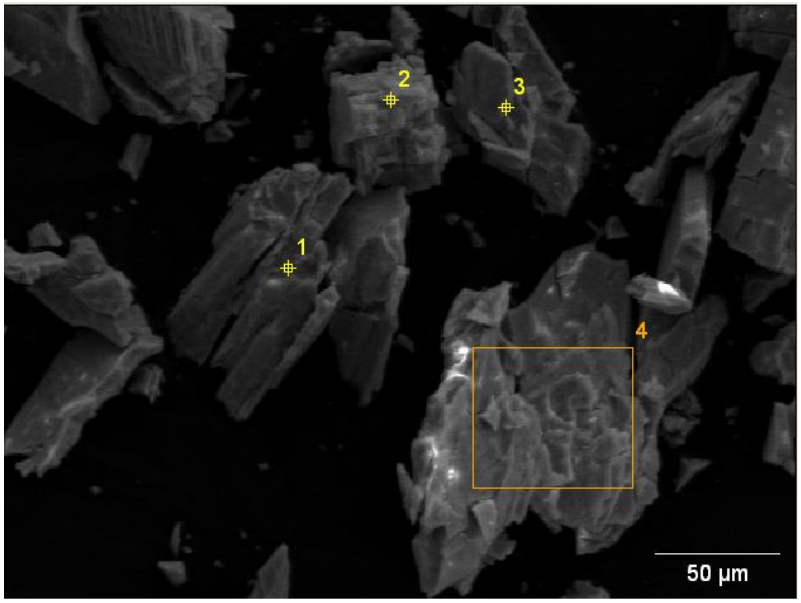

Fig. S12 The SEM image of the microcrystalline sample of **$Eu_{1.2}Tb_{0.8}Pt_3$** with the labelling of the points 1–3 and the area 4 targeted for the EDXMA experiment (see Table S18 for the results). The other representative SEM images for selected materials from the investigated family of **Ln_2M_3** (Ln = Eu, Tb; M = Pt, Pd) are shown in Figure 1 while the relate results of the EDXMA are gathered in Tables S18–S21.

Table S18 Results of SEM-EDXMA analysis of the rare earth metals composition in **$Eu_{1.2}Tb_{0.8}Pt_3$**.

metal	**Eu**	**Tb**
measured atomic compositions (only rare earth metals included, independent measurements) / %	59.40(1.31)	40.60(1.42)
	59.03(1.33)	40.97(1.42)
	62.18(1.39)	37.82(1.48)
	59.20(1.31)	40.80(1.41)
	58.19(1.27)	41.81(1.37)
	56.37(1.30)	43.63(1.39)
	62.11(0.83)	37.89(1.48)
	60.41(1.32)	39.59(1.42)
	58.35(1.30)	41.65(1.40)
	56.10(1.34)	43.90(1.45)
average atomic composition (only rare earth metals included) / %	59.13(1.27)	40.87(1.42)
relative atomic composition (only rare earth metals included, calculated for 3 Pt centers)	**1.18**	**0.82**
Eu/Tb metal ratio (found)	1.4(2)	
proposed metal composition	**1.2**	**0.8**
Eu/Tb metal ratio (calculated)	1.5	

Table S19 Results of SEM-EDXMA analyses of the rare earth metals composition in **$Eu_{1.2}Tb_{0.8}Pd_3$** and **$Eu_{0.6}Tb_{1.4}Pt_3$**.

metal	Eu	Tb
$Eu_{1.2}Tb_{0.8}Pd_3$		
measured atomic composition (only rare earth metals included, independent measurements)[a] / %	56.12(0.95)	43.88(1.03)
	57.46(0.92)	42.54(0.99)
	57.25(1.0)	42.75(1.08)
	58.23(0.8)	41.77(0.86)
	55.18(0.86)	44.82(0.93)
average atomic composition (only rare earth metals included) / %	56.82(0.91)	43.18(0.98)
relative atomic composition (only rare earth metals included, calculated for 3 Pd centers)	**1.14**	**0.86**
Eu/Tb metal ratio (found)	1.3(2)	
proposed metal composition	**1.2**	**0.8**
Eu/Tb metal ratio (calculated)	1.5	
$Eu_{0.6}Tb_{1.4}Pt_3$		
measured atomic composition (only rare earth metals included, independent measurements)[a] / %	30.47(0.81)	69.53(1.72)
	30.99(1.5)	69.01(1.73)
	30.11(1.44)	69.89(1.70)
	25.89(1.39)	74.11(1.67)
	27.93(0.83)	72.07(1.77)
	30.08(1.58)	69.92(1.84)
	30.28(1.43)	69.72(1.69)
	30.48(0.81)	69.52(1.68)
	26.62(1.5)	73.38(1.78)
average atomic composition (only rare earth metals included) / %	29.10(1.31)	70.90(1.73)
relative atomic composition (only rare earth metals included, calculated for 3 Pt centers)	**0.58**	**1.42**
Eu/Tb metal ratio (found)	0.41(6)	
proposed metal composition	**0.6**	**1.4**
Eu/Tb metal ratio (calculated)	0.43	

Table S20 Results of SEM-EDXMA analyses of the rare earth metals composition in **$Eu_{0.6}Tb_{1.4}Pd_3$** and **$Eu_{0.4}Tb_{1.6}Pt_3$**.

metal	**Eu**	**Tb**
$Eu_{0.6}Tb_{1.4}Pd_3$		
measured atomic composition (only rare earth metals included, independent measurements)[a] / %	32.87(1.22)	67.13(1.43)
	31.06(0.59)	68.94(1.26)
	30.98(1.01)	69.02(1.21)
	30.89(1.01)	69.11(1.22)
	29.05(0.98)	70.95(1.19)
	34.38(0.67)	65.62(1.41)
average atomic composition (only rare earth metals included) / %	31.61(0.91)	68.39(1.29)
relative atomic composition (only rare earth metals included, calculated for 3 Pd centers)	**0.64**	**1.36**
Eu/Tb metal ratio (found)	0.46(6)	
proposed metal composition	**0.6**	**1.4**
Eu/Tb metal ratio (calculated)	0.43	
$Eu_{0.4}Tb_{1.6}Pt_3$		
measured atomic composition (only rare earth metals included, independent measurements)[a] / %	20.51(1.18)	79.49(1.45)
	20.68(0.56)	79.32(1.55)
	18.36(0.96)	81.64(1.19)
	20.27(0.55)	79.73(1.12)
	20.07(0.53)	79.93(1.19)
	19.55(0.54)	80.45(1.21)
	23.73(0.61)	76.27(1.33)
	20.99(0.66)	79.01(1.51)
	22.30(0.67)	77.70(1.51)
average atomic composition (only rare earth metals included) / %	20.72	79.28
relative atomic composition (only rare earth metals included, calculated for 3 Pt centers)	**0.41**	**1.59**
Eu/Tb metal ratio (found)	0.26(3)	
proposed metal composition	**0.4**	**1.6**
Eu/Tb metal ratio (calculated)	0.25	

Table S21 Results of SEM-EDXMA analysis of the rare earth metals composition in **$Eu_{0.4}Tb_{1.6}Pd_3$**.

metal	**Eu**	**Tb**
measured atomic composition (only rare earth metals included, independent measurements)[a] / %	18.80(0.41)	81.20(0.94)
	19.17(0.83)	80.83(1.06)
	20.37(0.8)	79.63(1.03)
	22.61(0.45)	77.39(1.01)
	17.96(0.7)	82.04(0.89)
	18.19(0.73)	81.81(0.92)
	19.71(0.75)	80.29(0.95)
	20.07(0.81)	79.93(1.03)
average atomic composition (only rare earth metals included) / %	19.63(0.69)	80.37(0.98)
relative atomic composition (only rare earth metals included, calculated for 3 Pt centers)	**0.39**	**1.61**
Eu/Tb metal ratio (found)	0.24(3)	
proposed metal composition	**0.4**	**1.6**
Eu/Tb metal ratio (calculated)	0.25	

Comment to Tables S18–S21

For each compound from the series of **$Eu_{1.2}Tb_{0.8}M_3$**, **$Eu_{0.6}Tb_{1.4}M_3$**, and **$Eu_{0.4}Tb_{1.6}M_3$** (M = Pt, Pd), EDXMA (energy dispersive X-ray microanalysis) analyses were conducted on a few different single crystals and a few places of the selected single crystal (see Fig. 1 and S12). The results of atomic compositions of Eu and Tb metal centers were averaged. The obtained average atomic compositions included only rare earth metals, and they were used to estimate the relative metal composition. It was calculated assuming three Pt centers for the formula of each compound, according to the crystal structures (Fig. 1 and Tables S1–S3). Relative atomic composition values were rounded which resulted in the proposed metal composition. These proposed metal compositions were used to determine the full formula of the respective compounds, taking into account the results of CHN elemental analyses (see Experimental section). The identical methodology was previously used by us for heterometallic cyanido-bridged coordination clusters.[S5]

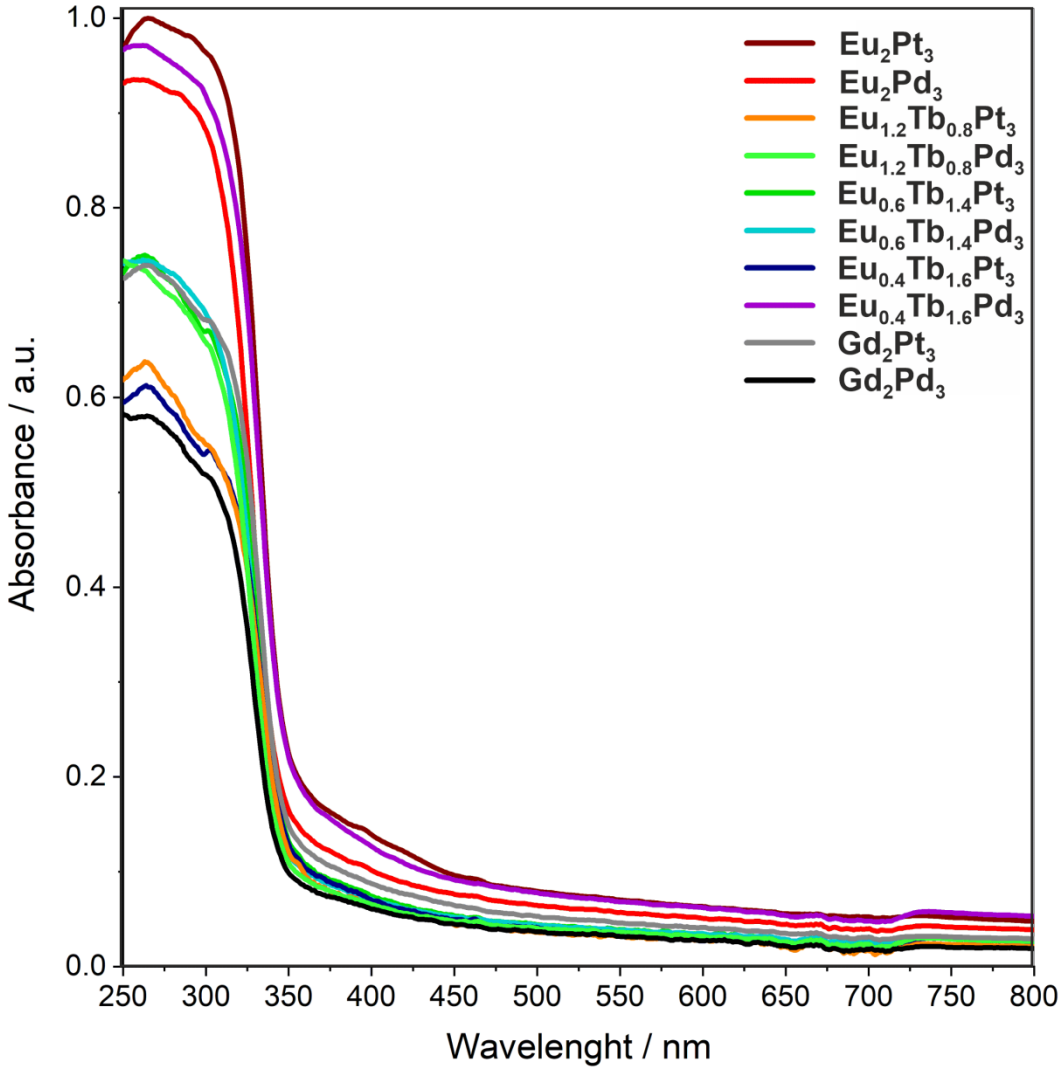

Fig. S13 UV-vis-NIR solid-state absorption spectra of $\mathbf{Eu_2M_3}$, $\mathbf{Eu_{1.2}Tb_{0.8}M_3}$, $\mathbf{Eu_{0.6}Tb_{1.4}M_3}$, $\mathbf{Eu_{0.4}Tb_{1.6}M_3}$, and $\mathbf{Gd_2M_3}$ (M = Pt, Pd) materials.

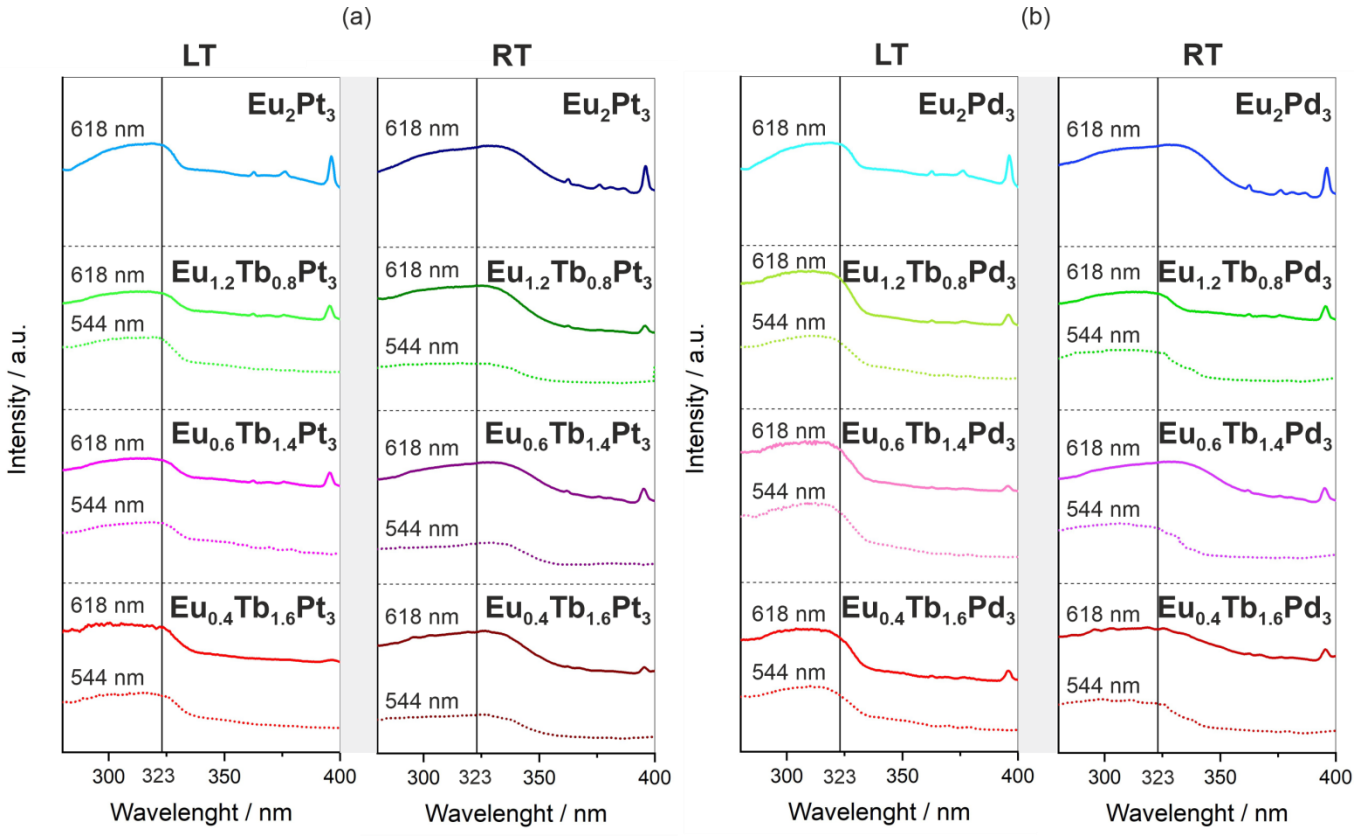

Fig. S14 Low- (LT, 77 K) and room- (RT, 298 K) temperature excitation spectra of Pt^{II}-containing compounds, **Eu_2Pt_3**, **$Eu_{1.2}Tb_{0.8}Pt_3$**, **$Eu_{0.6}Tb_{1.4}Pt_3$**, **$Eu_{0.4}Tb_{1.6}Pt_3$** (a), and their Pd^{II}-containing analogues, **Eu_2Pd_3**, **$Eu_{1.2}Tb_{0.8}Pd_3$**, **$Eu_{0.6}Tb_{1.4}Pd_3$**, and **$Eu_{0.4}Tb_{1.6}Pd_3$** (b) for the monitored emission wavelengths of 544 nm (Tb^{III} emission) and 618 nm (Eu^{III} emission). The 323 nm excitation wavelength, selected for the optical thermometric characteristics, was indicated by black vertical lines.

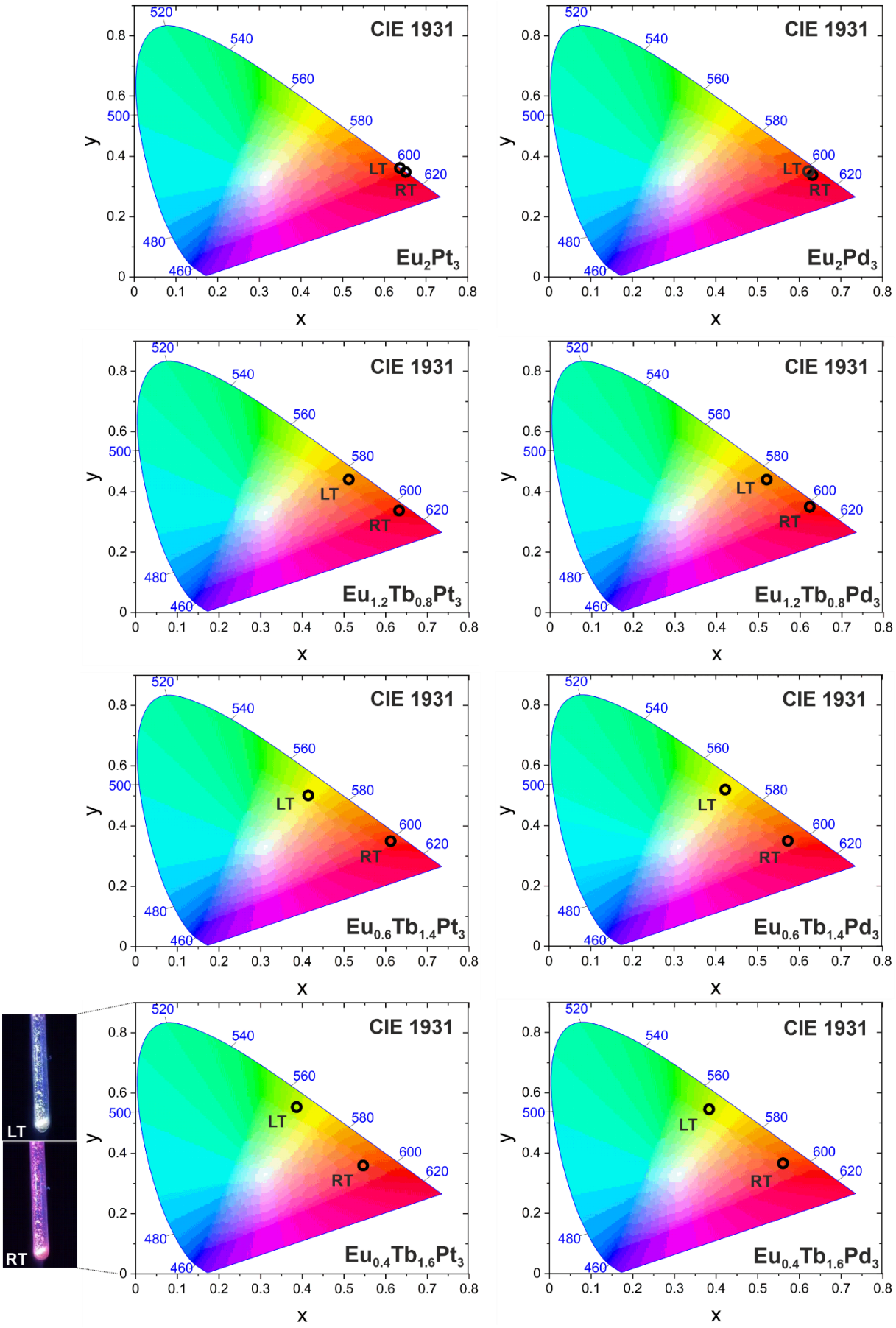

Fig. S15 Low- (LT, 77 K) and room- (RT, 298 K) temperature emission under the 323 nm excitation of $\mathbf{Eu_2M_3}$, $\mathbf{Eu_{1.2}Tb_{0.8}M_3}$, $\mathbf{Eu_{0.6}Tb_{1.4}M_3}$, and $\mathbf{Eu_{0.4}Tb_{1.6}M_3}$ (M = Pt, Pd), shown on the CIE 1931 chromaticity diagrams. For $\mathbf{Eu_{0.4}Tb_{1.6}Pt_3}$, the illustrative photos of emission at LT and RT were additionally presented.

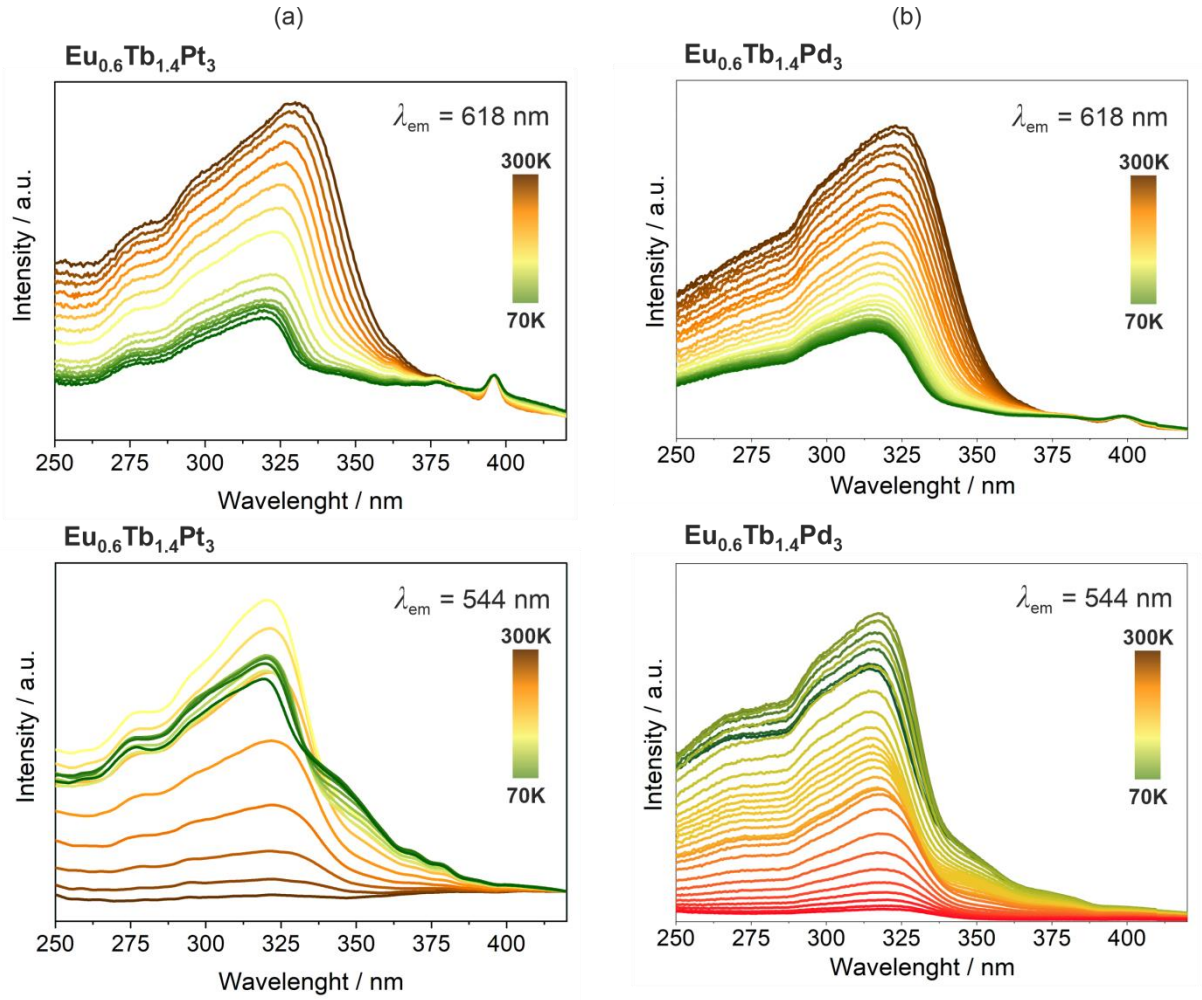

Fig. S16 Temperature dependences of excitation spectra of **$Eu_{0.6}Tb_{1.4}Pt_3$** (a) and **$Eu_{0.6}Tb_{1.4}Pd_3$** (b) in the 70-300 K temperature range, for two indicated monitored emission wavelengths of 618 nm (Eu^{III} emission) and 544 nm (Tb^{III} emission).

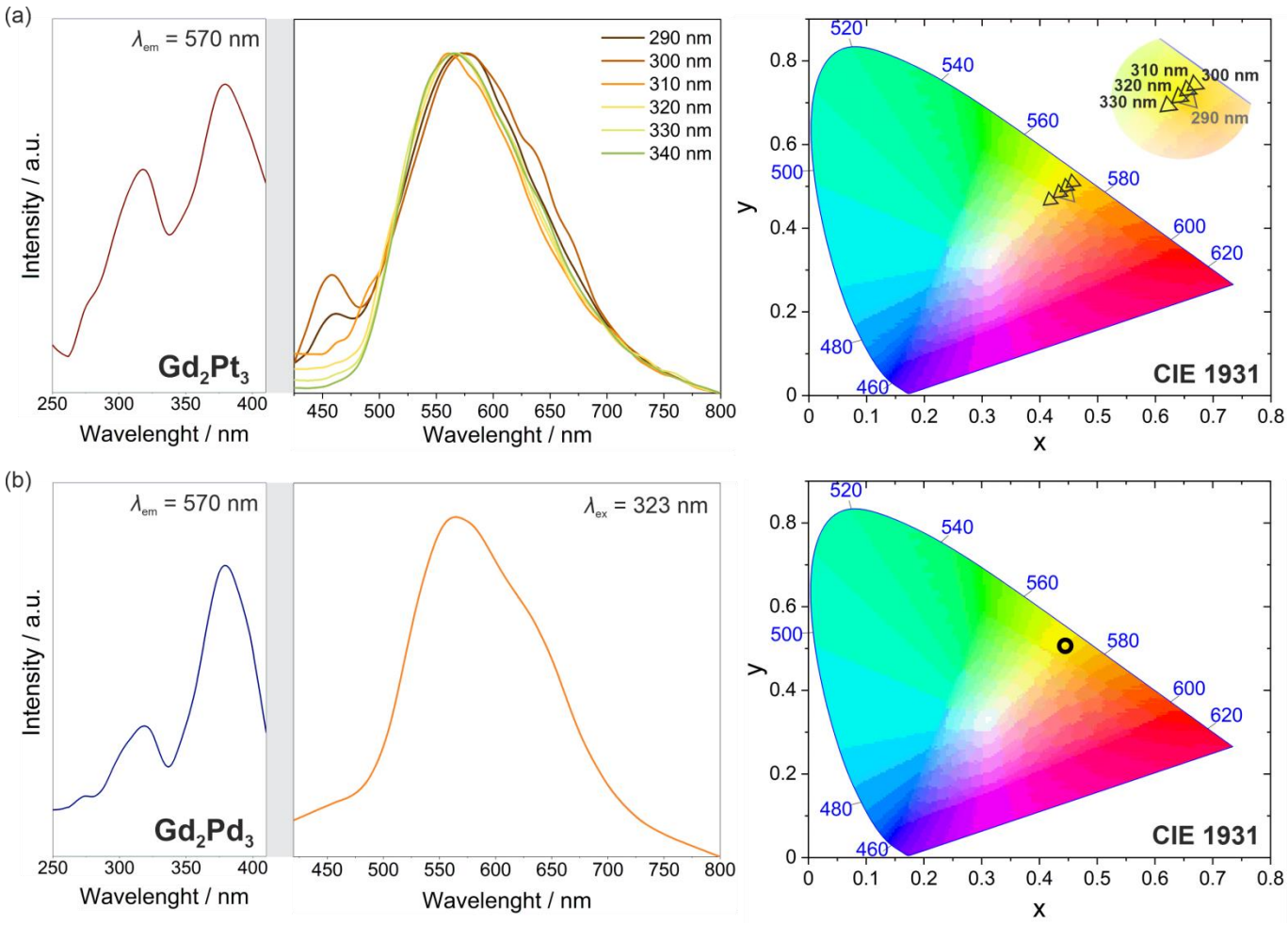

Fig. S17 Photoluminescence characteristics of **Gd_2Pt_3** (a) and **Gd_2Pd_3** (b) including excitation spectra for the monitored emission at 570 nm (left side), emission spectra for the indicated excitation wavelengths (central panel), and the related emission colours shown on the CIE 1931 chromaticity diagrams (right side). Note that the excitation-dependent emission spectra are shown for **Gd_2Pt_3** only as the **Gd_2Pd_3** analog does not show any dependence of the emission pattern on the excitation wavelength.

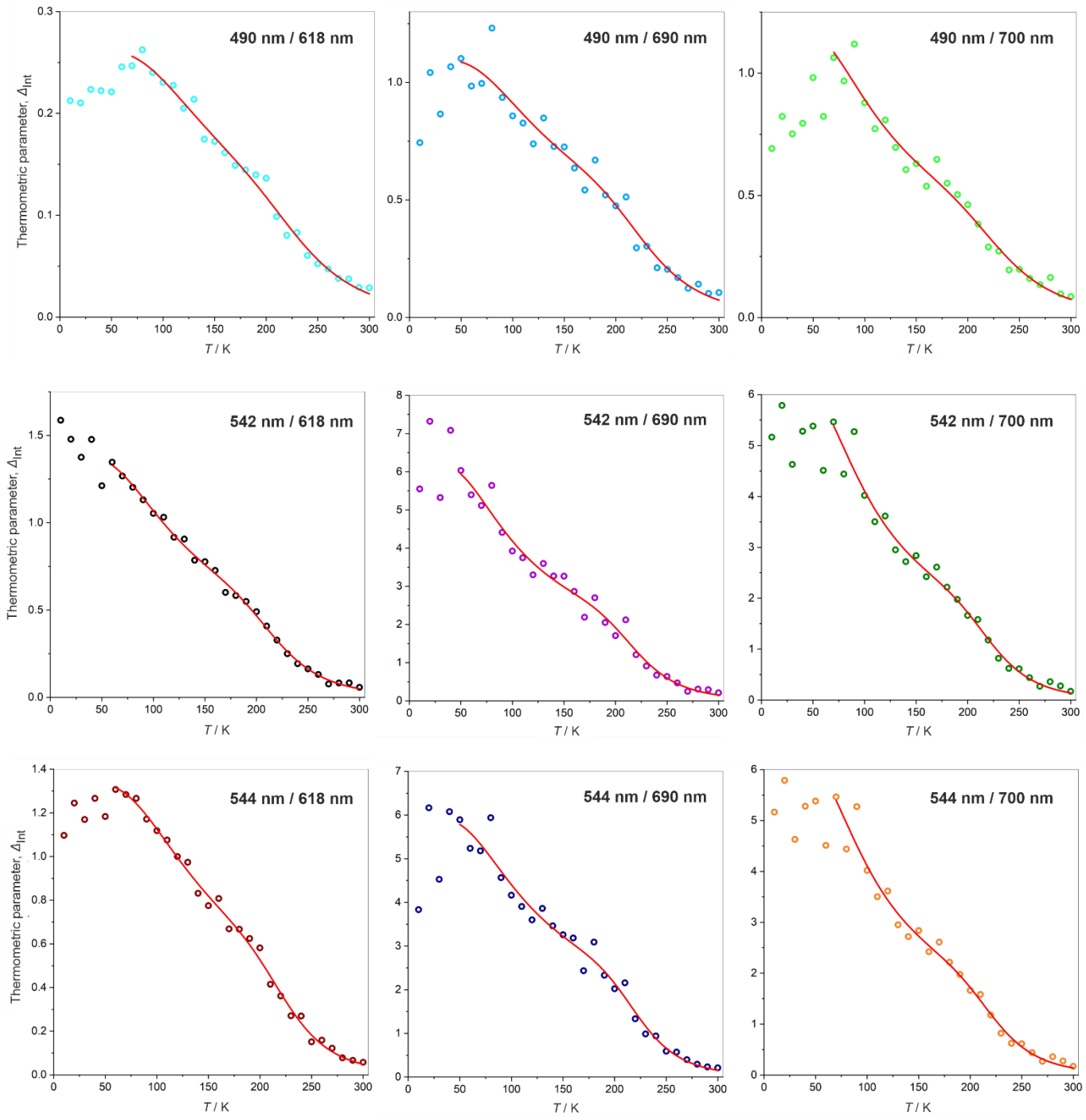

Fig. S18 Temperature dependences of the thermometric parameters, Δ_{Int} (empty circles points), of **$Eu_{0.6}Tb_{1.4}Pt_3$**, defined as the ratios between emission intensities for the indicated emission wavelengths related to the Tb^{III} emission (490, 542, or 544 nm) and the Eu^{III} emission (618, 690, or 700 nm), shown together with the best-fit curves (solid lines) according to the Mott-Seitz involving two-non-radiative recombination channels (see equation 2 and Fig. 4 of the main text, and Table S22 below).

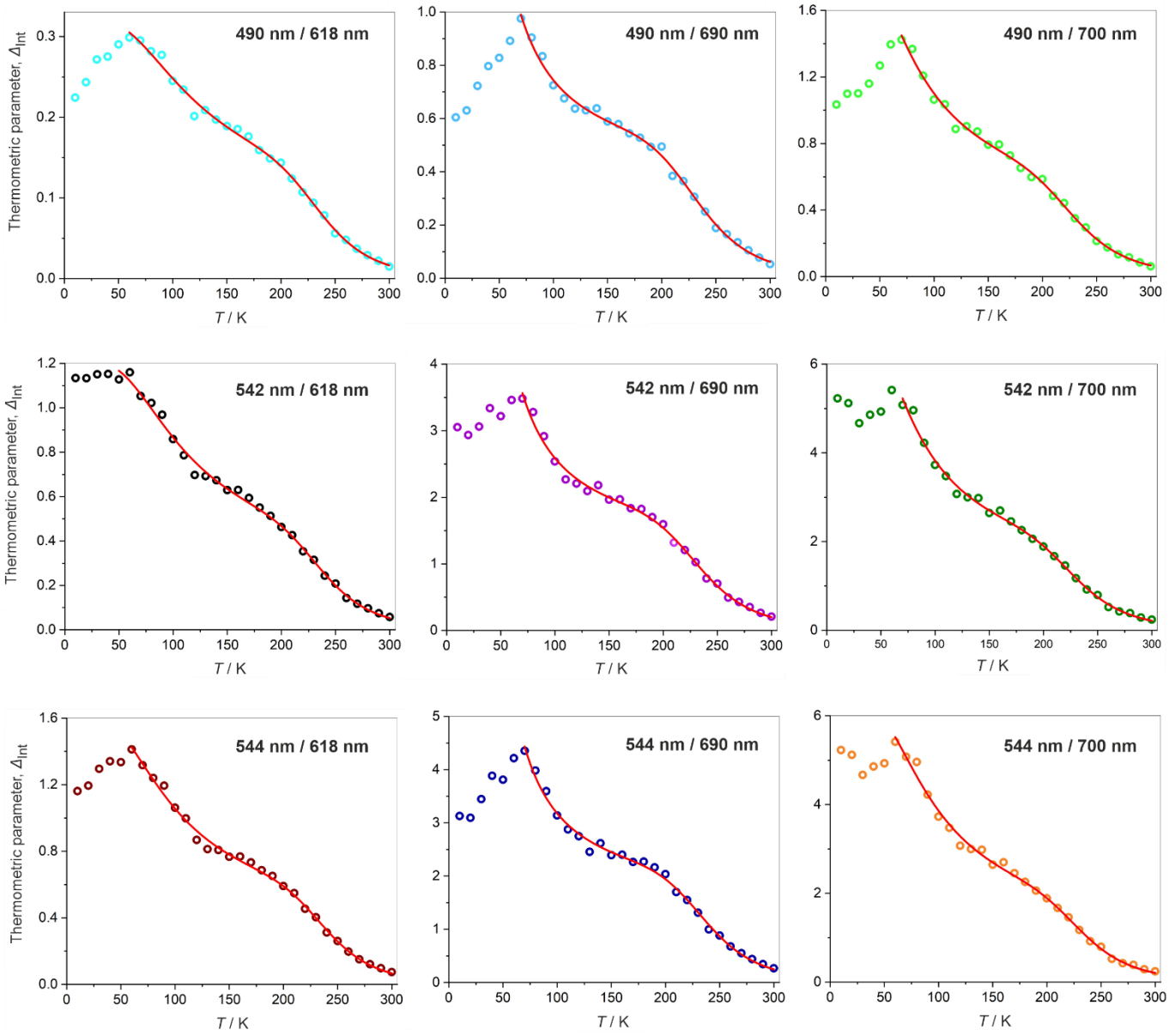

Fig. S19 Temperature dependences of the thermometric parameters, Δ_{Int} (empty circles points), of **$Eu_{0.6}Tb_{1.4}Pd_3$**, defined as the ratios between emission intensities for the indicated emission wavelengths related to the Tb^{III} emission (490, 542, or 544 nm) and the Eu^{III} emission (618, 690, or 700 nm), shown together with the best-fit curves (solid lines) according to the Mott-Seitz involving two-non-radiative recombination channels (see equation 2 and Fig. 4 of the main text, and Table S22 below).

Table S22 Best-fit parameters for the temperature-dependences of emission-intensity-based thermometric parameters, Δ_{Int}, for **$Eu_{0.6}Tb_{1.4}Pt_3$** and **$Eu_{0.6}Tb_{1.4}Pd_3$**, according to the Mott-Seitz model involving two-non-radiative recombination channels (see equation 2 and main text for details, and Fig. S18–S19 for comparison). The thermometric parameters are defined as the ratios between the emission intensities at the indicated emission wavelengths.

Wavelengths for the intensity ratio	Δ_0	$\Delta E_1/k_B$ / K	$\Delta E_2/k_B$ / K	α_1	α_2	R^2
$Eu_{0.6}Tb_{1.4}Pt_3$						
490 nm / 618 nm	0.262(3)	2004(24)	397(7)	6927(70)	6.7(3)	0.9894
490 nm / 690 nm	1.10(2)	2122(47)	306(1)	14500(300)	4.4(4)	0.9620
490 nm / 700 nm	1.20(2)	2082(42)	281(7)	13350(240)	5.6(3)	0.9733
542 nm / 618 nm	1.383(7)	2203(14)	301(3)	38530(240)	5.9 (1)	0.9975
542 nm / 690 nm	6.2(1)	2428(43)	238(6)	121610(230)	5.2(3)	0.9805
542 nm / 700 nm	6.3(1)	2493(46)	265(5)	165680(3350)	7.7(3)	0.9799
544 nm / 618 nm	1.33(1)	2474(20)	361(4)	93350(790)	7.0(2)	0.9955
544 nm / 690 nm	5.92(9)	2586(44)	263(8)	195680(3780)	4.8 (3)	0.9784
544 nm / 700 nm	6.3(1)	2493(46)	265(5)	165680(3340)	7.7(3)	0.9799
$Eu_{0.6}Tb_{1.4}Pd_3$						
490 nm / 618 nm	0.320(2)	2633(17)	264(3)	109170(7460)	4.1(1)	0.9960
490 nm / 690 nm	6.97(5)	2357(89)	76(3)	254400(1390)	17.9(7)	0.9958
490 nm / 700 nm	1.9(3)	2356(55)	183(4)	66700(670)	4.95(5)	0.9964
542 nm / 618 nm	1.20(3)	2680(32)	248(2)	150100(7800)	4.7(1)	0.9959
542 nm / 690 nm	28(8)	2397(44)	84(4)	363400(1170)	22.8(1)	0.9948
542 nm / 700 nm	7.6(4)	2406(28)	181.(3)	94620(640)	6.0(5)	0.9958
544 nm / 618 nm	1.60(7)	2744(28)	213(2)	195800(8530)	4.3(4)	0.9967
544 nm / 690 nm	26(8)	2531(88)	77(2)	266600(4720)	4.1(4)	0.9956
544 nm / 700 nm	6.3(3)	2529(32)	223(3)	123500(1590)	5.9(6)	0.9957

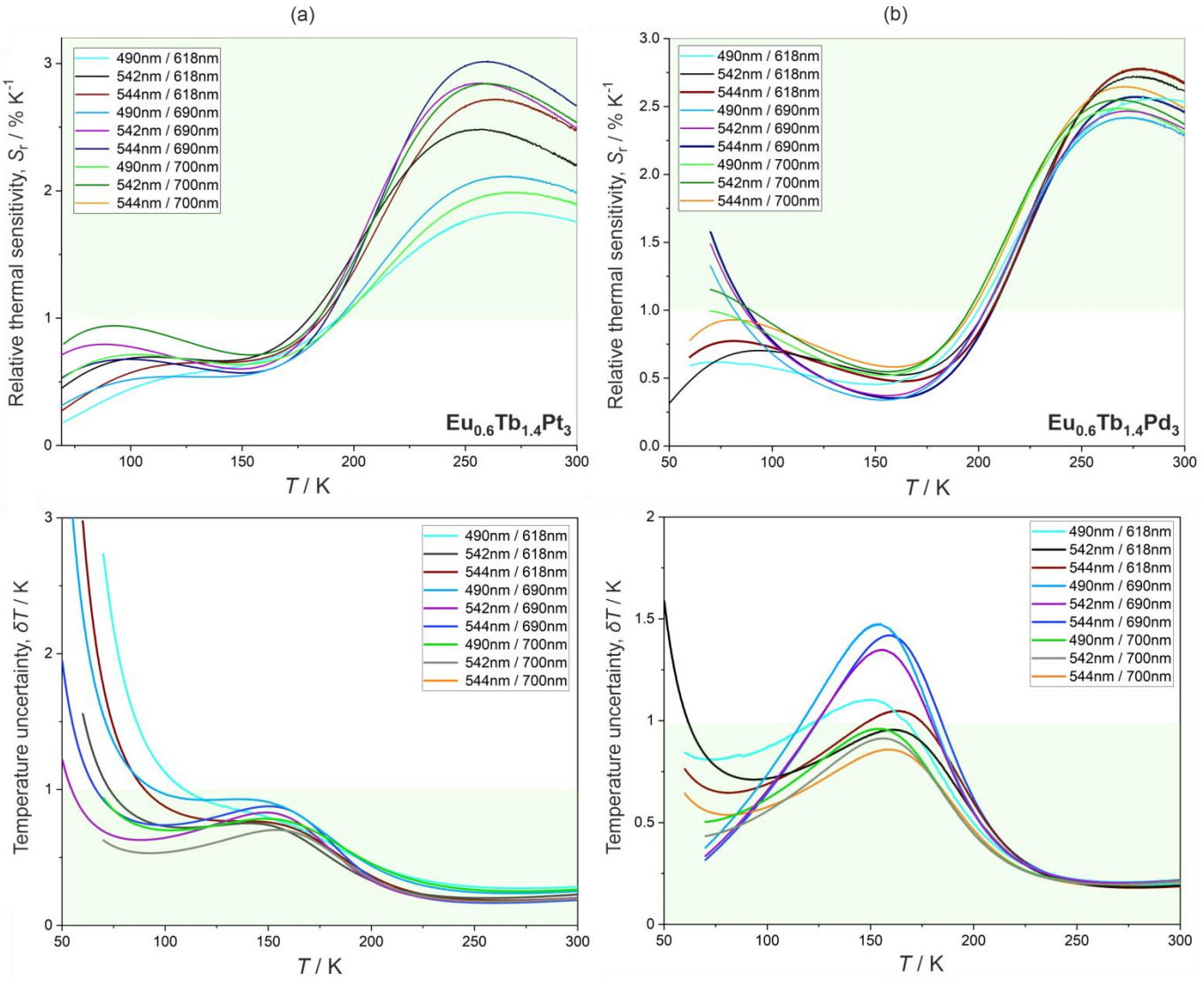

Fig. S20 Temperature dependences of relative thermal sensitivity (top part) and temperature uncertainty (bottom part) for the optical thermometric effects in **$Eu_{0.6}Tb_{1.4}Pt_3$** (a) and **$Eu_{0.6}Tb_{1.4}Pd_3$** (b), related to the emission intensity ratios determined using the emission peaks for various indicated pairs of emission wavelengths (see Fig. S18–S19 for comparison). Green areas represent the ranges of high-performance luminescent thermometry (S_r > 1% K^{-1} and δT < 1 K).

Table S23 Comparison of representative parameters of ratiometric emission-intensity-based luminescent thermometry for various examined thermometric parameters of **$Eu_{0.6}Tb_{1.4}Pt_3$** and **$Eu_{0.6}Tb_{1.4}Pd_3$** (Fig. S20), including the temperature ranges of the good thermometric performance (S_r > 1% K^{-1} and δT < 1 K) and the values of maximal thermal sensitivity.

thermometric parameter, Δ (T-range used for the fitting to the Mott-Seitz model)	**T / K range for S_r > 1% K^{-1} and δT < 1 K**	**maximal S_r (the related T)**
$Eu_{0.6}Tb_{1.4}Pd_3$		
Int_{490nm}/Int_{618nm} (60–300 K)	200–300 K	2.56% K^{-1} (T = 286 K)
Int_{542nm}/Int_{618nm} (60–300 K)	203–300 K	2.72% K^{-1} (T = 277 K)
Int_{544nm}/Int_{618nm} (60–300 K)	206–300 K	2.78% K^{-1} (T = 279 K)
Int_{542nm}/Int_{690nm} (70–300 K)	203–300 K	2.46% K^{-1} (T = 272 K)
Int_{490nm}/Int_{690nm} (70–300 K)	204–300 K	2.41% K^{-1} (T = 272 K)
Int_{544nm}/Int_{690nm} (70–300 K)	207–300 K	2.56% K^{-1} (T = 277 K)
Int_{490nm}/Int_{700nm} (70–300 K)	196–300 K	2.49% K^{-1} (T = 268 K)
Int_{542nm}/Int_{700nm} (70–300 K)	195–300 K	2.54% K^{-1} (T = 268 K)
Int_{544nm}/Int_{700nm} (60–300 K)	197–300 K	2.64% K^{-1} (T = 270 K)
$\tau_{544nm}/\tau_{618nm}$ (150–300 K)	193–300 K	3.04% K^{-1} (T = 255 K)
$Eu_{0.6}Tb_{1.4}Pt_3$		
Int_{490nm}/Int_{618nm} (70–300 K)	194–300 K	1.83% K^{-1} (T = 272 K)
Int_{542nm}/Int_{618nm} (60–300 K)	180–300 K	2.48% K^{-1} (T = 257 K)
Int_{544nm}/Int_{618nm} (60–300 K)	186–300 K	2.72% K^{-1} (T = 263 K)
Int_{542nm}/Int_{690nm} (50–300 K)	184–300 K	2.84% K^{-1} (T = 257 K)
Int_{490nm}/Int_{690nm} (50–300 K)	193–300 K	2.11% K^{-1} (T = 267 K)
Int_{544nm}/Int_{690nm} (50–300 K)	188–300 K	3.01% K^{-1} (T = 259 K)
Int_{490nm}/Int_{700nm} (70–300 K)	194–300 K	1.99% K^{-1} (T = 271 K)
Int_{542nm}/Int_{700nm} (70–300 K)	184–300 K	2.84% K^{-1} (T = 259 K)
Int_{544nm}/Int_{700nm} (70–300 K)	184–300 K	2.84% K^{-1} (T = 258 K)
$\tau_{544nm}/\tau_{618nm}$ (150–300 K)	181–300 K	3.26% K^{-1} (T = 239 K)

Table S24 Results of the fitting of emission lifetimes of $\mathbf{Eu_{0.6}Tb_{1.4}Pt_3}$ based on the experimental data collected at various temperatures under the 323 nm excitation, using the fitting model of the monoexponential decay function (see equation 1 and Fig. 5).

T / K	τ / µs	error	x^2	τ / µs	error	x^2
	λ_{em} = 544 nm (Tb^{III} emission)			λ_{em} = 618 nm (Eu^{III} emission)		
300	18.18	0.01	1.033	201.78	0.54	1.189
290	22.97	0.14	1.178	199.13	0.55	1.197
280	35.02	0.19	1.053	195.80	0.65	1.193
270	46.15	0.24	1.017	201.25	0.44	1.168
260	62.04	0.29	1.129	200.65	0.52	1.192
250	91.58	0.36	1.093	205.86	0.45	1.071
240	111.81	0.58	1.203	198.83	0.89	1.168
230	166.35	0.82	1.217	208.68	0.85	1.102
220	250.60	0.81	1.060	210.26	0.91	1.200
210	314.97	1.09	1.147	211.52	0.67	1.183
200	385.45	1.29	1.154	209.92	0.66	1.158
190	464.74	1.29	1.151	204.79	0.82	1.156
180	516.28	1.32	1.195	206.02	0.79	1.175
170	542.40	1.32	1.192	198.55	1.09	1.117
160	566.11	1.83	1.193	197.25	1.06	1.181
150	581.66	2.15	1.195	204.20	0.82	1.174
130	582.06	1.85	1.255	210.96	0.88	1.113
110	572.79	3.30	1.192	220.29	1.01	1.041
90	560.40	1.11	1.181	229.60	1.22	1.184
70	569.51	1.49	1.099	234.05	1.35	1.094
50	564.00	1.52	1.153	235.75	1.39	1.017
30	599.93	1.61	1.173	248.00	0.94	1.000
10	578.98	1.81	1.181	235.11	1.35	1.030

Table S25 Results of the fitting of emission lifetimes of **$Eu_{0.6}Tb_{1.4}Pd_3$** based on the experimental data collected at various temperatures under the 323 nm excitation, using the fitting model of the monoexponential decay function (see equation 1 and Fig. 5).

***T* / K**	**τ / µs**	**error**	**x^2**	**τ / µs**	**error**	**x^2**
	λ_{em} = 544 nm (Tb^{III} emission)			**λ_{em} = 618 nm (Eu^{III} emission)**		
300	34.71	0.22	1.143	199.38	0.65	1.138
290	44.34	0.40	1.092	207.08	0.49	1.166
280	58.06	0.40	1.092	209.43	0.43	1.147
270	79.79	0.51	1.132	211.22	0.38	1.107
260	95.98	0.91	1.136	214.69	0.43	1.181
250	119.41	0.98	1.126	215.13	0.50	1.095
240	182.55	1.05	1.117	219.36	0.45	1.123
230	222.37	2.83	1.021	222.37	0.76	1.103
220	314.48	1.69	1.189	223.05	0.67	1.198
210	373.84	1.97	1.097	222.45	0.68	1.153
200	469.69	1.76	1.225	225.51	0.77	1.182
190	512.02	1.20	1.089	226.55	0.62	1.102
180	550.70	2.01	1.152	227.17	0.69	1.258
170	563.90	2.07	1.110	230.79	0.76	1.119
160	573.91	2.14	1.113	228.93	0.72	1.175
150	583.69	2.79	1.067	228.63	0.66	1.180
140	588.55	2.94	1.093	228.91	0.69	1.163
130	588.97	2.57	1.116	228.94	0.82	1.150
110	594.11	4.64	1.030	233.94	0.65	1.182
90	479.60	1.62	1.143	240.23	0.81	1.160
70	554.07	1.41	0.998	255.20	1.05	1.098
50	575.93	1.53	1.129	257.72	0.89	1.145
30	560.39	1.581	1.050	255.86	0.95	1.228
10	557.67	2.27	0.985	255.82	0.98	1.202

Table S26 Emission lifetimes for various compounds from the investigated series of **$Eu_{1.2}Tb_{0.8}M_3$**, **$Eu_{0.6}Tb_{1.4}M_3$**, and **$Eu_{0.4}Tb_{1.6}M_3$** (M = Pt, Pd), based on the experimental data collected at 77 K (LT) and 298 K (RT) under the 323 nm excitation, determined using the fitting model of the monoexponential decay function.

compound	τ / µs	error	x^2	τ / µs	error	x^2
	λ_{em} = 544 nm (Tb^{III} emission)			λ_{em} = 618 nm (Eu^{III} emission)		
LT, 77 K						
$Eu_{1.2}Tb_{0.8}Pt_3$	549.88	1.06	1.06	238.63	0.41	1.09
$Eu_{1.2}Tb_{0.8}Pd_3$	517.11	1.38	1.20	230.01	0.74	1.06
$Eu_{0.6}Tb_{1.4}Pt_3$	569.51	1.49	1.10	234.05	1.35	1.09
$Eu_{0.6}Tb_{1.4}Pd_3$	529.98	1.41	1.21	236.80	1.63	1.04
$Eu_{0.4}Tb_{1.6}Pt_3$	567.17	1.33	1.11	273.96	1.47	1.04
$Eu_{0.4}Tb_{1.6}Pd_3$	520.97	1.94	1.26	249.34	1.56	1.05
RT, 298 K						
$Eu_{1.2}Tb_{0.8}Pt_3$	16.22	0.03	1.23	219.37	0.20	1.12
$Eu_{1.2}Tb_{0.8}Pd_3$	19.52	0.11	1.29	214.76	0.25	1.04
$Eu_{0.6}Tb_{1.4}Pt_3$	18.18	0.10	1.03	201.18	0.52	1.19
$Eu_{0.6}Tb_{1.4}Pd_3$	25.81	0.11	1.47	210.23	0.56	1.03
$Eu_{0.4}Tb_{1.6}Pt_3$	17.74	0.19	1.21	214.10	0.19	1.09
$Eu_{0.4}Tb_{1.6}Pd_3$	26.89	0.09	1.38	210.83	0.45	0.93

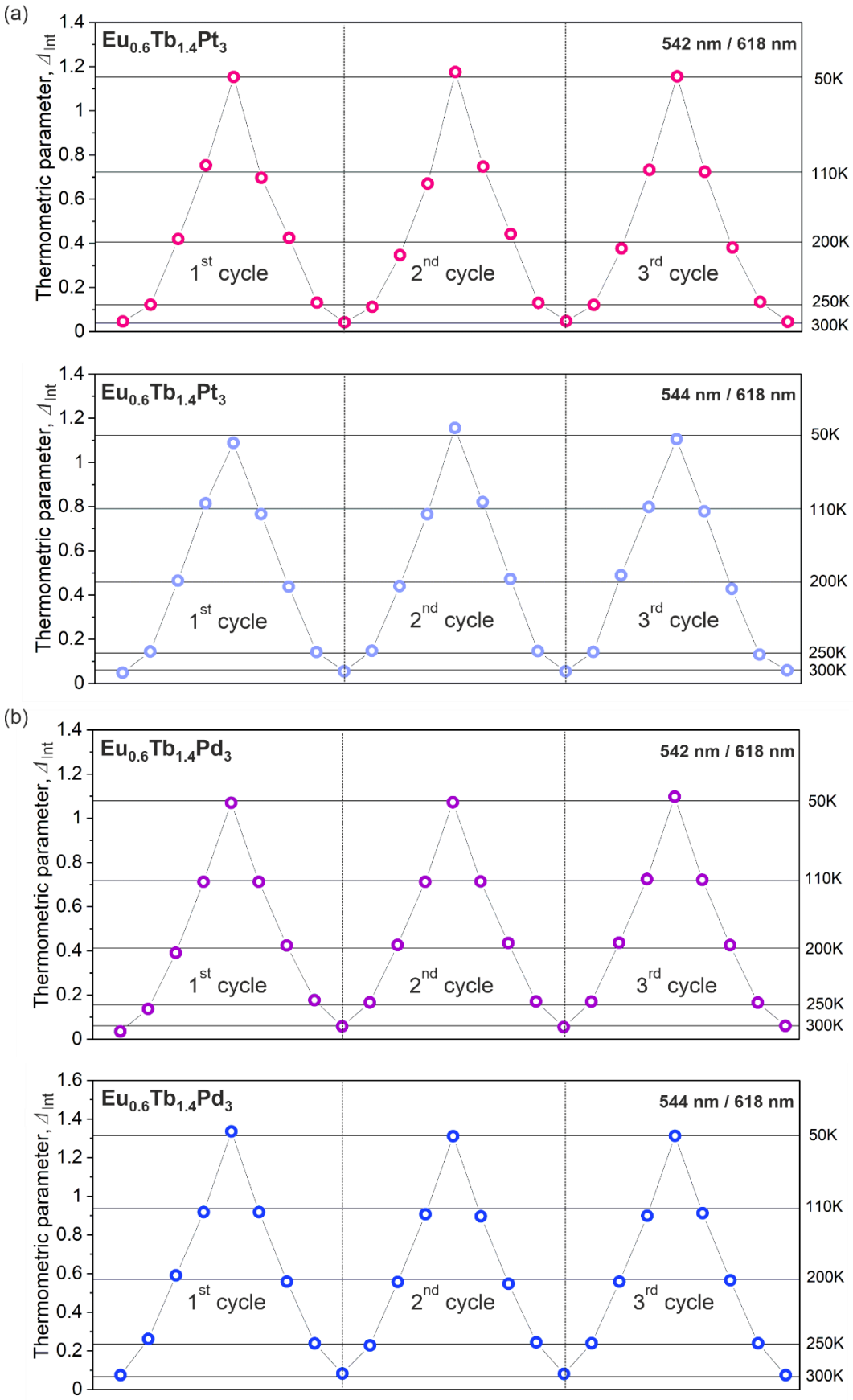

Fig. S21 Changes in thermometric parameters, Δ_{Int}, defined as the ratios between emission intensities for the indicated pairs of emission wavelengths under the 323 nm excitation (see Fig. 4), occurring upon the temperature cycling between 300 and 50 K (three indicated cycles of cooling and heating) for **$Eu_{0.6}Tb_{1.4}Pt_3$** (a) and **$Eu_{0.6}Tb_{1.4}Pd_3$** (b). The resulting repeatability of the thermometric behavior is above 96% for both compounds.

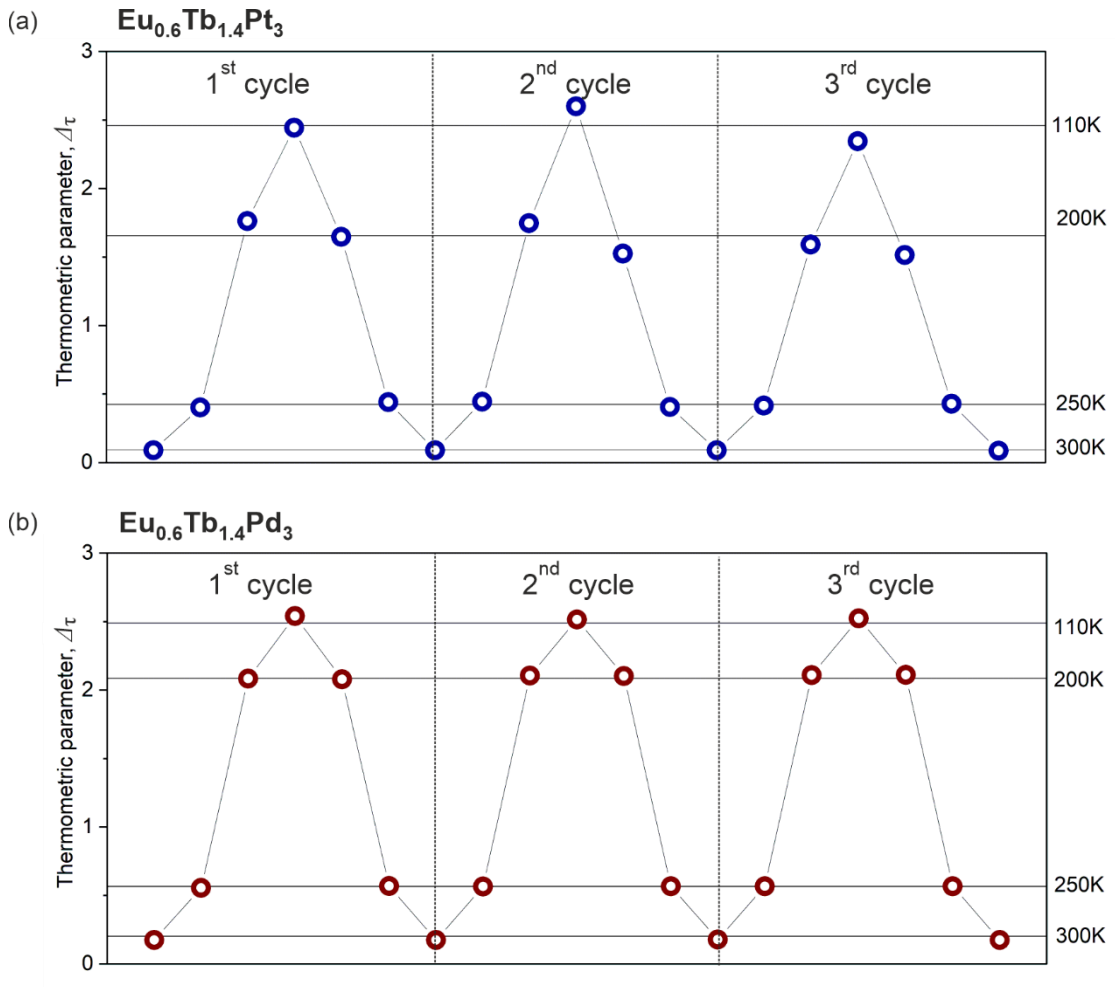

Fig. S22 Changes in thermometric parameters, Δ_τ, defined as the ratio between emission lifetimes for the emission peaks at 544 nm and 618 nm upon the 323 nm excitation (see Fig. 5), occurring upon the temperature cycling between 300 and 50 K (three indicated cycles of cooling and heating) for **$Eu_{0.6}Tb_{1.4}Pt_3$** (a) and **$Eu_{0.6}Tb_{1.4}Pd_3$** (b). The resulting repeatability of the thermometric behavior is above 96% for both compounds.

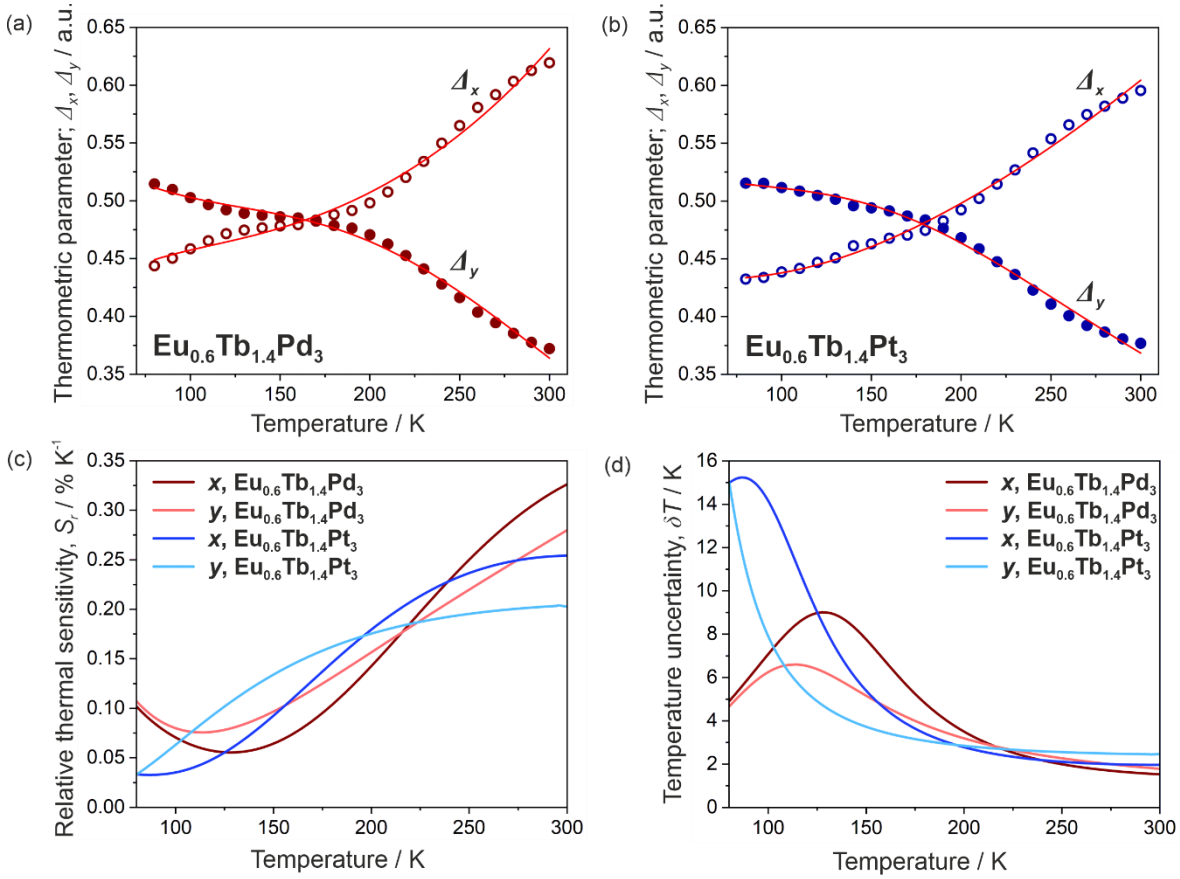

Fig. S23 Representative characteristics of the alternative optical thermometric effect in **$Eu_{0.6}Tb_{1.4}Pt_3$** and **$Eu_{0.6}Tb_{1.4}Pd_3$**, exploring the *x* and *y* parameters (CIE 1931 chromaticity scale) of the emission colours (Fig. 4c) as the thermometric parameters, Δ_x and Δ_y, respectively. In (a), the $\Delta_x(T)$ and $\Delta_y(T)$ dependences for **$Eu_{0.6}Tb_{1.4}Pd_3$** was shown while the analogous curves for **$Eu_{0.6}Tb_{1.4}Pt_3$** were presented in (b). Coloured points in (a) and (b) represent the experimental data obtained tracing the position of the overall emission on the CIE 1931 chromaticity diagram while solid lines are the best-fit curves to the Mott-Seitz model (equation 2, main text; best-fit parameters of $\Delta E/k_B$ are 759(6) K and 3.1(2) K for Δ_x in **$Eu_{0.6}Tb_{1.4}Pd_3$**, 1200(7) K and 31(1) K for Δ_y in **$Eu_{0.6}Tb_{1.4}Pd_3$**, 855(5) K and 86(9) K for Δ_x in **$Eu_{0.6}Tb_{1.4}Pt_3$**, 462(4) K and 3(1) K for Δ_y in **$Eu_{0.6}Tb_{1.4}Pt_3$**). The (c) part contains the temperature dependences of the resulting relative thermal sensitivity values (equation 1, main text) whereas the (d) part contains the temperature dependences of resulting temperature uncertainty values (equation 4, main text). The curves in (c) and (d) were obtained using the best-fit curves of the $\Delta_x(T)$ and $\Delta_y(T)$ dependences.

References to Supporting Information

(S1) B. A. Maynard, P. A. Smith, L. Ladner, A. Jaleel, N. Beedoe, C. Crawford, Z. Assefa and R. E. Sykora, Emission Enhancement through Dual Donor Sensitization: Modulation of Structural and Spectroscopic Properties in a Series of Europium Tetracyanoplatinates, *Inorg. Chem*., 2009, **48**, 6425–6435.

(S2) P. A. Smith, C. Crawford, N. Beedoe, Z. Assefa and R. E. Sykora, Synthesis, Crystal Structures, and Dual Donor Luminescence Sensitization in Novel Terbium Tetracyanoplatinates, *Inorg. Chem*., 2012, **51**, 12230–12241.

(S3) M. Llunell, D. Casanova, J. Cirera, J. Bofill, P. Alemany, S. Alvarez, M. Pinsky and D. Avnir, *SHAPE v. 2.1, Program for the Calculation of Continuous Shape Measures of Polygonal and Polyhedral Molecular Fragments*; University of Barcelona: Barcelona, 2013.

(S4) D. Casanova, J. Cirera, M. Llunell, P. Alemany, D. Avnir and S. Alvarez, Minimal Distortion Pathways in Polyhedral Rearrangements, *J. Am. Chem. Soc*., 2004, **126**, 1755–1763.

(S5) M. Liberka, J. Kobylarczyk, T. M. Muziol, S. Ohkoshi, S. Chorazy and R. Podgajny, A heterotrimetallic synthetic approach of nanosized $\{M_xCu_{13-x}W_7\}^{3+}$ and $\{M_1Cu_8W_6\}$ (M = Co, Ni, Mn, Fe) metal–cyanide magnetic clusters, *Inorg. Chem. Front*., 2019, **6**, 3104–3118.